J Intell Robot Syst (2015) 78:257–289
DOI 10.1007/s10846-014-0061-6

Development and Control of a Multifunctional Prosthetic Hand with Shape Memory Alloy Actuators

Konstantinos Andrianesis · Anthony Tzes

Received: 19 November 2013 / Accepted: 8 April 2014 / Published online: 25 May 2014

Abstract In this research paper, non-conventional actuation technology, based on shape memory alloys, is employed for the development of an innovative low-cost five-fingered prosthetic hand. By exploiting the unique properties of these alloys, a compact, silent and modular actuation system is implemented and integrated in a lightweight and anthropomorphic rapid-prototyped hand chassis. A tendon-driven underactuated mechanism provides the necessary dexterity while keeping the mechanical and control complexity of the device low. Tactile sensors are integrated in the fingertips improving the overall hand control. Embedded custom-made electronics for hand interfacing and control are also presented and analyzed. For the position control of each digit, a novel resistance feedback control scheme is devised and implemented. The functionality and performance of the developed hand is demonstrated in grasp experiments with common objects.When compared to the current most advanced commercial devices, the technology applied in this prototype provides a series of improvements in terms of size, weight, and noise, which will enable upper limb amputees to carry out their basic daily tasks more comfortably.

Keywords Upper limb prosthetics · Multifingered hands · Underactuated robots · Smart actuators · Shape memory alloys · Resistance feedback control

Mathematics Subject Classifications (2010) 68T40

Electronic supplementary material The online version of this article (doi:10.1007/s10846-014-0061-6) contains supplementary material, which is available to authorized users.

K. Andrianesis · A. Tzes (✉)
Department of Electrical and Computer Engineering, University of Patras, Rio, Greece
e-mail: tzes@ece.upatras.gr

K. Andrianesis
e-mail: kandrianesis@ece.upatras.gr

1 Introduction

Much effort over the last years has been involved in the creation of advanced robotic hands imitating the functionality and form of their biological counterpart. Inspired by the dexterity and versatility of the human hand, scientists from all over the world strive towards the development of more anthropomorphic manipulators. Some impressive devices have already been demonstrated such as the Shadow Hand [1], DLR Hand [2] and NASA/JPL Robonaut Hand [3]. These hands can be employed in various application fields such as in automation, tele-manipulation, humanoid robotics and space exploration. However, when it comes to prosthetics, these hands fail to operate successfully, since different physical constraints, challenging trade-offs and strict criteria must be met in order to be acceptable by their users. These criteria have already been disclosed in several publications

[4–8] and include humanlike appearance, compactness, low weight and cost, silent operation and the ability to form a competent number of prehension patterns useful in performing most of the activities of daily living (ADLs); as expected, the compromise of these demanding specifications leads to less dexterous devices than the previously cited state-of-the-art robotic hands.

In the early 1970s, motorized prosthetic hands with one degree of freedom (DOF) became commercially available. These were basically simple grippers with two rigid fingers in opposition to a rigid thumb, and hence with poor grasping capabilities [9]. Recently, commercialized hand prostheses have seen a significant improvement with the introduction to the market of novel multi-articulated designs, capable of different grasping patterns. In 2007, i-Limb hand (Touch Bionics, Inc.) was the first-to-market prosthesis with five individually-powered digits and a manually rotatable thumb. Few years later, the Michelangelo hand (Ottobock, Inc.) and the Bebionic hand (RSL Steeper, Inc.) were also introduced with similar features. In 2013, the latest revision of the i-Limb hand (i-Limb Ultra Revolution) possessing a powered rotating thumb has become available [10]. Several research laboratories have also demonstrated impressive multifunctional devices for prosthetic purposes. Some of the most recent notable efforts include the SmartHand [11], and the full prosthetic arm created by DEKA [12] within the framework of DARPA's Revolutionizing Prosthetics program.

Although all these hands are a major breakthrough compared to the previous status of the electrically powered prostheses with the single-DOF devices, they are still insufficient to fulfil all the aforementioned needs of their users. In particular, issues concerning their weight, cost and noise levels are some of the major shortfalls that lead to lower user satisfaction and acceptance rates. All these issues are strongly related with the limitations imposed from the conventional direct-current (DC) electric motors utilized for their actuation. Despite the widespread use of these actuators in a large range of applications, they undergo drastic reductions in power as they are scaled down; as a consequence, bulky, heavy and noisy driving systems with increased manufacturing costs are requisite. Other traditional actuators such as hydraulic and pneumatic actuators, which are much lighter than electric motors for the same power capability, have been investigated - e.g. the Fluidhand [13] - but have other limitations such as a complex system of pumps and valves, and a requirement for compressed air to operate.

Therefore, finding alternative types of actuation becomes critical for enhancing prosthesis functionality and acceptance. Towards this goal, a large variety of non-conventional actuators have already been investigated as potential candidates for the next generation of upper limb prostheses. Thorough review papers and comparative studies have also been published [14–16]. One of the most promising of these actuators concerns the utilization of Shape Memory Alloys (SMAs) and in particular Nickel-Titanium (NiTi) alloys (or Nitinol). These are smart materials that have the ability to return to their predetermined shape when heated above a certain transition temperature. This property (known as shape memory effect) is due to a solid-state phase transformation from the martensite form to the austenite form [17]. During this transformation, if SMAs encounter any external resistance, they can yield ample actuation forces. Their most commonly used form involves inexpensive thin cylindrical wires optimized to contract like muscles when heated. These actuator wires present an incredibly high power-to-weight ratio and can be easily driven by electrical current via ohmic heating. Additional assets include a cost-effective inherent position feedback method (given a relationship between electrical resistance and strain) and silent operation. The latter feature is particularly important in prosthetic applications wherein users do not want to attract attention when operating their prostheses.

Robotic hand designs employing SMA wires as actuators have already been disclosed in a few publications. DeLaurentis and Mavroidis presented an early prototype of a 20-DOF hand designed to be actuated by bundles of SMA wires [18, 19]. Maeno and Hino developed a miniature five-fingered robotic hand for dexterous manipulation of small tissues and parts in medical and industrial fields [20]. Cho, Rosmarin and Asada demonstrated a five-fingered robotic hand with 16 controlled DOFs and SMA wires divided into 32 independently joule-heated segments [21]. Jung, Bae and Moon have proposed a lightweight SMA underactuated hand with five digits and only 6 controlled DOFs [22]. Lee, Okamoto and Matsubara have recently developed and tested a hand prototype with a fixed thumb and four fingers, actuated by SMA wires

installed inside the fingers [23]. Moreover, some other research groups have experimented with preliminary finger setups [24–28] and grippers [29–31].

To the authors' knowledge, there is still no compact and practical device presented in the engineering literature that employs SMA actuators and can be envisioned as a true prosthetic aid for upper limb amputees. The limiting factors that hindered till now the successful integration of these actuators in prosthetic applications are mostly related to strain, efficiency, speed and control issues [4, 14]. The main objective of this research work is to mitigate these issues with the appropriate techniques and methods and devise an innovative prosthetic hand by effectively exploiting the competitive advantages of the SMAs.

The following sections present the design, fabrication and control of an anthropomorphic, multifunctional and compact prosthetic hand with SMA actuators. The prosthetic hand system described herein is the outcome of a number of years of research [32–35], whereby each of its aspect has been explored to fulfil most of the needs of the prostheses users. The structure of the remainder of this paper is as follows. Section 2 describes the mechanical design and physical implementation of the hand chassis. Section 3 presents the development and integration of the SMA actuation system and electronics within the hand envelope. In Section 4, control experiments with a single-finger testbed are presented, while the performance of the self-contained hand prototype is evaluated in grasp experiments of everyday objects. Finally, Section 5 summarizes and discusses the contribution of this paper and gives an outlook on future work.

2 Prototype Development

Considering the current technological means, the human hand still represents an immensely challenging benchmark for every designer. Its functional uniqueness arises from a complex geometric arrangement of joints, tendons and muscles enabling a massive array of movements and uses. Although it is not in the scope of this research work to develop an anatomical copy of the human hand, a comprehensive study of its physiology was conducted. Through the functional understanding of the human hand, it is easier to derive the guidelines for the design of a multifunctional yet compact prosthetic device with anthropomorphic appearance.

The human hand consists of many small bones called carpals, metacarpals and phalanges (Fig. 1). The carpals are located in the wrist, the metacarpals form the palm, and the phalanges constitute the skeleton of the fingers and thumb [36]. The four fingers (index, middle, ring and little) have similar structure, with each of them containing three phalanges: the distal phalanx, carrying the nail, the medial (or intermediate) phalanx, and the proximal phalanx. These phalanges are connected by two 1-DOF hinge joints, called interphalangeal joints (IP joints), allowing flexion/extension movements. The joint near the fingertip is called the distal IP joint (DIP joint) while the other one is called the proximal IP joint (PIP joint). Unlike the fingers, the thumb contains only two phalanges and consequently only one IP joint. All digits (fingers and thumb) connect to their corresponding metacarpals through condyloid 2-DOF joints, called metacarpophalangeal joints (MCP joints or knuckles). These joints, which are treated ideally as saddle or universal joints [37], permit flexion/extension as well as limited abduction/adduction movements. The motion of the thumb is also dictated by another joint, its carpometacarpal (CMC) joint, found at the base of its metacarpal bone. This joint has two non-orthogonal and non-intersecting rotation axes [38] and can be considered as a 2-DOF saddle joint. It produces flexion/extension and abduction/adduction motion and based on its geometry enables thumb opposition, one of the primary factors of the versatility and dexterity

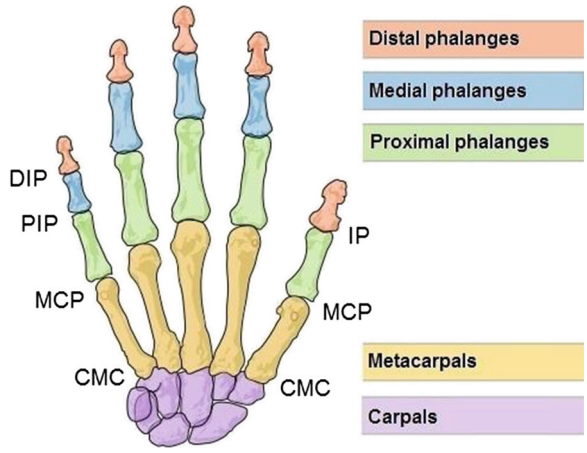

Fig. 1 Bones and joints of the (*right*) human hand [40]

of the human hand [36]. On the contrary, the CMC joints of the finger metacarpals have very limited motion capability. More specifically, the metacarpals of the index and middle fingers are fixed, while the metacarpals of the ring and little fingers are free to move in a small range enabling palm curving; an important feature for some grasping tasks. In total, the human hand alone has at least 17 joints and 23 DOFs [39].

Joint motion is produced by contractile forces exerted by muscles located in the forearm (extrinsic muscles) and palm (intrinsic muscles). These forces are transferred to the bones of the digits via flexible and strong connective tissues, known as tendons. Due to tendon connections, the forces generated by the muscles are translated into torques about the hand joints. Since muscles are only able to exert pulling effort, antagonistic (i.e. opposing) muscle pairs are employed for moving these joints. The extrinsic muscles are able to transfer force not only to a single joint but also to several joints due to a convoluted network of interdependently acting tendons - this sophisticated tendon arrangement contributes to the high functionality of human hand. These muscles are large and provide the necessary strength for flexion (flexor muscles) and extension (extensor muscles) of the digits. On the other hand, the intrinsic muscles are small and weaker, and used for adduction/abduction and other precision movements of the digits. Thus, whereas the extrinsic contribution resulting from the large powerful forearm muscle groups is more important to hand strength, the fine precision action imparted by the intrinsic musculature gives the hand an enormous variety of capabilities [41].

2.1 General Design Specifications

Based on the above study of the human hand physiology and taking into consideration the requirements of the upper limb prostheses users, an SMA actuated anthropomorphic prosthetic hand was designed (Fig. 2). The selection of its characteristics and specifications was determined by trade-offs between dexterity, complexity, size and weight. In order to retain hand compactness, the actuators and electronics are remotely located in a small-sized forearm structure, as shown in the CAD representation of Fig. 3. Similarly to the human hand, drive transmission is achieved through the use of artificial tendons (further details about the implemented transmission type will be discussed later).

The shape and size of the proposed hand prosthesis was designed to be anatomically consistent with that of an average human hand. Specifically, its dimensions, shown in Fig. 4, were extrapolated from anthropometric hand data for a 50th percentile US female [42]. The digits of the prosthetic hand, presented in Fig. 4 in their fully extended position, are mounted on the palm section with fixed inclinations and they are easily removable when necessary with just unscrewing the corresponding bolts, hence allowing ease of maintenance and service. The hand opening (i.e. the distance between the tips of the thumb and index finger) is also illustrated to be equal to 135.8 mm. This

Fig. 2 CAD model of the prosthetic hand in different views

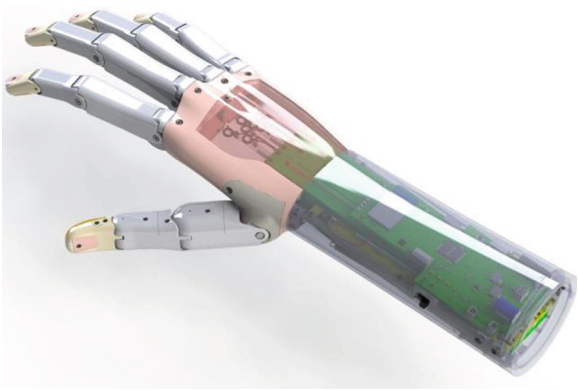

Fig. 3 Self-contained hand model with translucent covers

exceeds by far the 100 mm limit, suggested by Weir and Sensinger [43] in order an artificial hand to be able to grasp everyday objects like beverage cans. It is noted that the current most advanced commercial prosthetic hands, such as the i-Limb, have the same hand opening as the current design, allowing for grasps of large-volume objects to be performed.

Special care was taken in the design of the palm. Inspired by the human hand and the grasp stability that its arches provide [44], a cambered palm was designed as it is illustrated in Fig. 5. Unlike other hand prostheses which incorporate conventional voluminous actuators into their palms, the presented prosthetic hand takes advantage of its remotely located actuators in order to improve the anthropomorphic characteristics of its palm structure.

2.2 Kinematic Design

One of the key challenges in the prosthetic hand design concerns the definition of its kinematic structure. In order to allow the reproduction of the most common grasping types of the human hand, a high number of DOFs was chosen to be implemented as shown in Fig. 6. Each digit comprises three hingedly connected segments and thereby three DOFs. In total, the hand integrates fifteen (15) 1-DOF joints named after the corresponding ones (CMC, MCP, IP, PIP, DIP) of the human hand, albeit not exact analogues. Compared to the human archetype, the abduction/adduction motion of the MCP joints is not implemented in this design since it would adversely affect the shape, size and mechanism simplicity. For the same reason, the CMC joints of the ring and little fingers are omitted**.** Regarding the thumb, its CMC

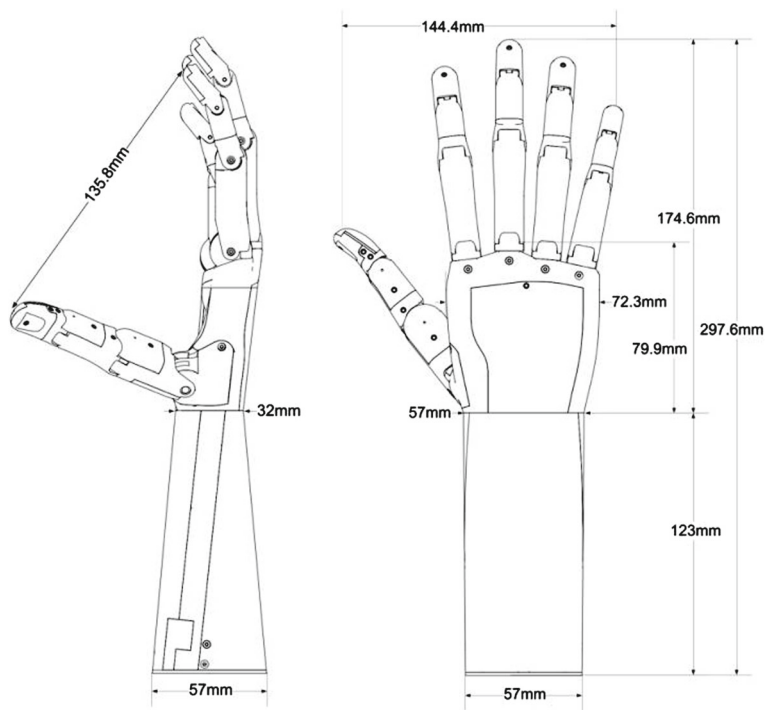

Fig. 4 Dimensions of the prosthetic hand

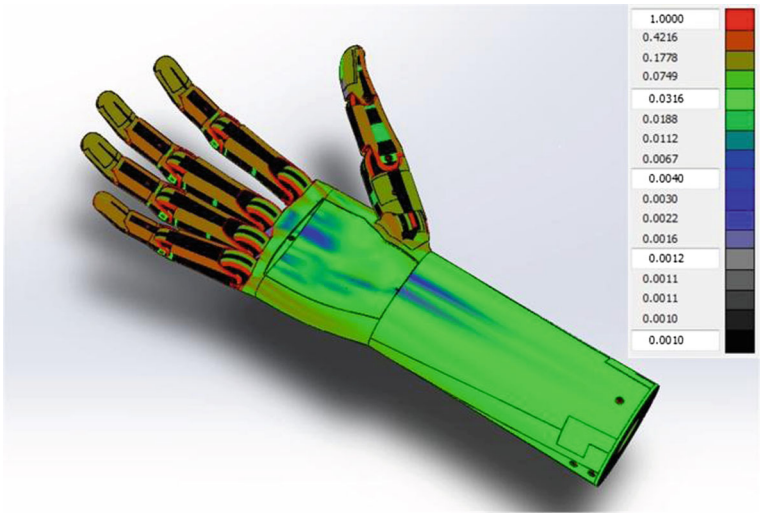

Fig. 5 Curvature of the prosthetic hand shown on a *black-to-red scale*. *Black color* illustrates totally flat surfaces

joint is simplified to a 1-DOF joint permitting only abduction/adduction movements. It is noted that setting up the location and orientation of the axis of this joint was one of the most challenging tasks and several designs were evaluated to ensure proper thumb functionality.

Due to the restricted weight and space criteria of our design, only a limited number of actuators can be accommodated in the structure. Therefore, an underactuation concept was exploited, wherein a number of DOFs is controlled with less number of actuators, yet allowing each digit to move separately. Specifically, as shown in Fig. 6, each finger was designed to have two underactuated controllable joints (MCP/PIP) and one passive DIP joint. The thumb was also designed to have a pair of underactuated controllable joints (MCP/IP) and additionally one independently controllable joint (CMC).

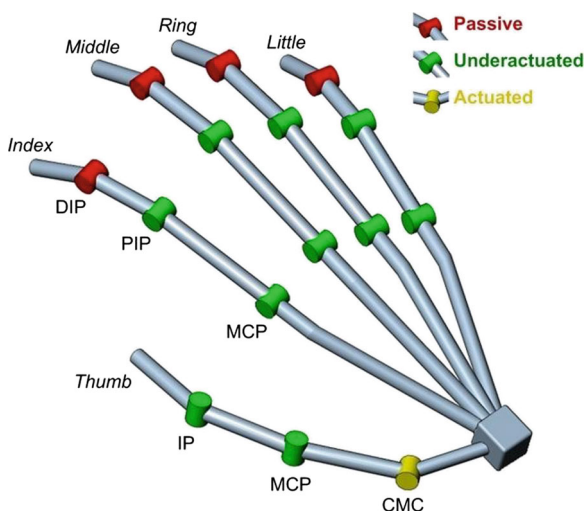

Fig. 6 Kinematic structure of the prosthetic hand

This underactuated mechanism allows the prosthetic hand to grasp objects of various sizes and shapes by passively adapting to their geometry (adaptive grasp), in a manner similar to the manner in which the digits of a human hand grasp and hold such objects. Thus, the final position of each digit is defined by the geometric characteristics of the grasped object. Underactuated mechanisms have already been extensively studied and implemented successfully in several artificial hands – e.g. the Laval hands [45, 46].

In order to transmit forces from the actuators to the moving links of the prosthetic hand, a tendon-based system is used. The biological inspiration suggests that this type of transmission system is beneficial. Indeed, many prehension devices have already adopted tendon-based systems for minimizing their transmission dimensions and weight, reducing setup and maintenance costs and offering a gentler grasping compared to other types such as linkages or gears [47]. In this research work, artificial tendons made of nylon-coated stainless steel cables are employed in order to propagate the actuation to the controllable joints of the hand. These cables were opted due to their high stiffness, flexibility and low friction. As it will be shown in the following section, they are guided by means of pulleys, placed in the joints of each digit, ensuring the necessary torque is provided no matter the posture of the digit.

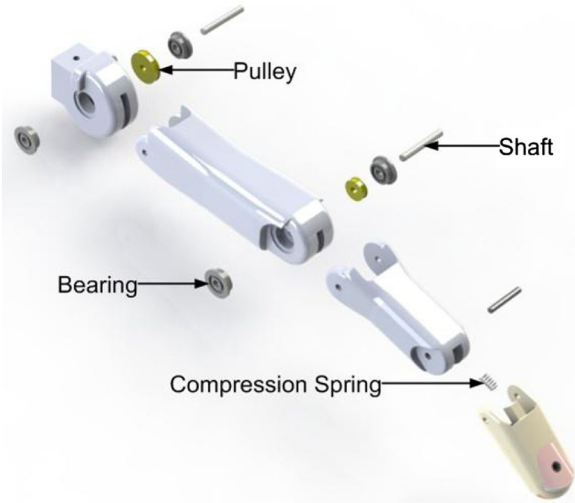

Fig. 7 Exploded view of a representative finger

2.3 Fingers Design

Each finger is constructed in substantially the same manner. It consists of three "phalanges" (this term is intentionally selected for describing the links of the fingers as in the human hand), whose dimensions were determined using the anthropometric measurements found in [42] and the study of [48]. Some adaptations, however, were made to fit the design needs. Moreover, phalanges of different fingers which were estimated to be close in size are modeled as being identical with the same average dimensions. In this way, the number of different parts of the hand is reduced as well as its future manufacturing cost.

In Fig. 7, the main components of each finger are presented. The three phalanges (proximal, medial and distal) are interconnected with metal shafts of 2 mm diameter. Another shaft interconnects the proximal phalange to a finger mount (knuckle) secured to the palm section by means of a screw. In order to minimize friction, each shaft is supported by a pair of 6 mm outer diameter ball bearings, snapping into the corresponding finger apertures. All these three parallel-to-each-other shafts form the axes about which the finger phalanges rotate. Miniature brass idle pulleys were custom-fabricated and mounted on the shafts of the tendon-driven underactuated finger joints (MCP/PIP). DIP joint is passively flexed at 25 degrees via a small compression spring between the medial and distal phalange and thereby compliant fingertips are achieved for more stable grasps.

As it is shown in Fig. 8, finger actuation is achieved via a pair of opposing tendons: one for flexion - flexor tendon, and another for extension - extensor tendon, routed under and over the guidance pulleys, respectively. This bidirectional tendon system is necessary since tendons can only be used to pull. The one end of the extensor and flexor tendons, as it will be discussed in Section 3, is tied to an active or passive actuation device. The other end of these tendons is fixed in the medial phalange of the finger by means of low-profile securing devices. Each of these devices comprises a plastic tube and a screw, configured in such a way that slight adjustments of the tendon length can be easily implemented in order to compensate when necessary any tendon creep or slackening.

The range of motion (ROM) of these joints is summarized in Table 1. Analytically, in each finger, the MCP joint has a ROM from 0°(extension) to 100° (flexion) while the PIP joint from 15° to 90° (hence 75°ROM). The DIP joint, as already mentioned, can be passively extended up to 25°. The workspace of a representative finger (index) is drawn in Fig. 9. As it is shown, the working envelope is large enough in order to permit enclosing various objects of different sizes and it covers almost the same ROM of a human finger [36]. However, due to the underactuated mechanism employed in each finger, the different positions of the fingertip, which define the workspace of Fig. 9, can

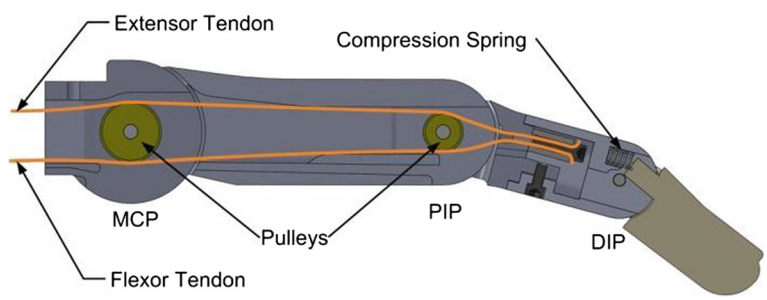

Fig. 8 Cross-sectional side view of a representative finger showing tendon routing

Table 1 Joint motion

	Joint	ROM	Type of Motion
Fingers	MCP	100º (0-100º)	Underactuated
	PIP	75º (15-90º)	Underactuated
	DIP	25º (0-25º)	Passive
Thumb	CMC	50º (0-50º)	Actuated
	MCP	90º (0-90º)	Underactuated
	IP	50º (0-50º)	Underactuated

only be achieved under the presence of certain external forces exerted by grasped objects or other external constraints.

On the other hand, in the absence of external forces, the fingertip trajectory is determined by the generated torques at the underactuated joints of the finger. More specifically, as it is already shown in Fig. 8, artificial tendons generate torque at the MCP and PIP joints by means of pulleys whose external diameters were selected to be 8 mm and 5 mm, respectively; this was an empirical selection dictated by the general need of having larger torque at the base joint of the finger [49] and taking into consideration the available force and displacement levels of the actuators (further details in Section 3.2). Assuming a constant tension in the extensor tendon, the extension torque produced in each joint is also constant since pulleys are always in contact with this tendon. On the contrary, the torque produced by the flexor tendon is variable. Instead of having this tendon wrapped around the pulleys for generating a constant torque amount, it was preferred to run it under the pulleys. In this way, the distance of the flexor tendon from each of the joint axes varies depending on the finger posture and the physical constraints of the finger interior. Apart from the obvious benefits in finger assembly, this way of tendon routing ensures that the fingertip trajectory follows the same path of Fig. 10 for both flexion and extension finger movements. As it shown, during flexion of the finger, the proximal phalange moves first and then the medial phalange motion takes place. In this way, fingers are able to curl around objects to form a stable grip. During opening of the hand (extension movements), fingers travel on the same pathway, with their phalanges having the reverse sequence of motion. It is noted that the finger trajectory is not significantly influenced from the gravity conditions since the weight of the finger phalanges is low and thus their torque contribution is negligible.

2.4 Thumb Design

Given the great importance of the thumb in the dexterity and versatility of the human hand, much design effort was expended in ensuring its high functionality in the proposed prosthetic device. Its structure differs substantially from the one shown previously in the fingers. It consists of three movable links patterned after human anatomy including two phalanges and a metacarpal segment. Their dimensions, though based on anthropometric data, are more of

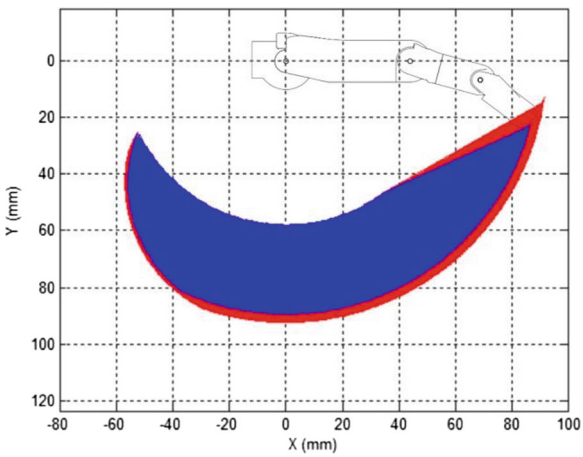

Fig. 9 Workspace of the index finger with (*red*) and without (*blue*) motion of the DIP joint. Finger scheme is depicted in its stretched out position

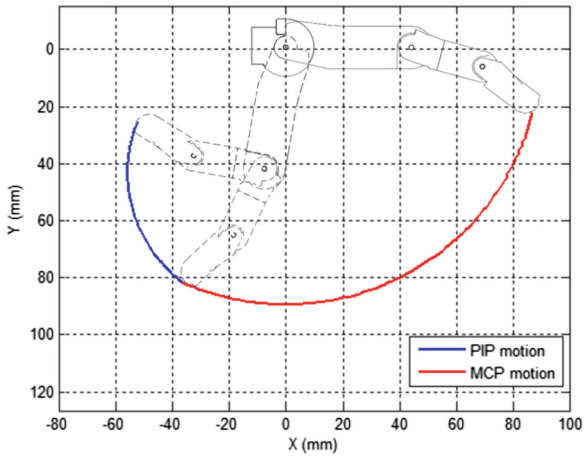

Fig. 10 Superimposed images of the index finger for three positions across the trajectory of its fingertip in the absence of external forces

the result of an iterative simulation process. Thumb assembly includes also a part, specifically designed to fit and secure to the palm section and connect with the metacarpal. Metal shafts are used for forming the joints of the thumb. In contrast with the fingers, only the axes of the last two joints of the thumb (MCP/IP) are parallel to each other while the axis of the CMC joint is placed perpendicular to them. The ROM of these joints can be found in Table 1. Figure 11 illustrates schematically the travel range of the CMC joint; this abduction motion combined with flexion of the other two joints moves thumb in opposition to the other fingers.

In Fig. 12, the thumb structure is presented with its joints at their stretched out position. The routing of the tendons is also shown in this figure. Specifically, the CMC joint employs only one tendon for its actuation along with a bias extension spring integrated between the proximal phalange and thumb mount. The MCP and IP joints use also a spring-biased scheme. Standard coil springs are properly arranged between the thumb phalanges providing a passive flexion force. However, besides an extensor tendon, a flexor tendon is also used in order to increase force exertion during grasping tasks. A pulley system having the exact same characteristics with the one found in the fingers is used for these two underactuated joints. Special care was taken to ensure that the routing of these tendons do not produce any torque in the CMC joint. This was achieved with metal guide shafts horizontally mounted into miniature bearings in the thumb mount. Bearings are also provided for all the joint shafts for limiting friction in tendon transmission.

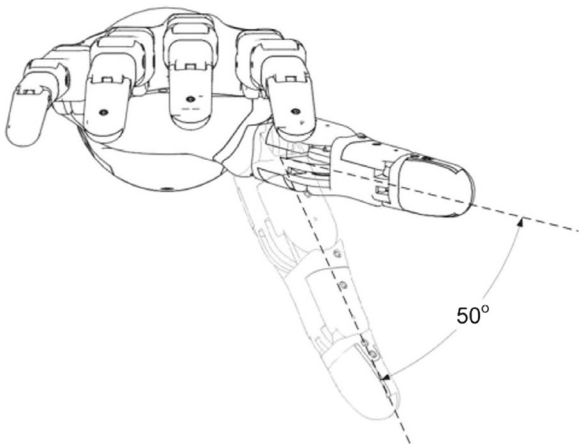

Fig. 11 Range of motion of the CMC thumb joint

2.5 Prototype Fabrication

The physical implementation of the hand design is realized using Selective Laser Sintering (SLS) process. SLS is an additive rapid prototyping process that builds rapidly three dimensional solid parts layer upon layer by using a laser to selectively sinter (heat and fuse) a powdered material [50]. In this research work, a fiber-reinforced plastic composite (Duraform HST) with high strength and stiffness was used for building each of the components of the hand chassis.

Once the different CAD-generated solid parts were built, the chassis of the prosthetic hand was assembled with the help of the other critical components (screws, shafts, bearings, etc.). Its mass is about 160 grams and as it will be discussed later, after the integration of the actuators and electronics, the whole hand prototype is estimated to weigh significantly less than the current commercial solutions. The dorsal and palmar views of the assembled hand chassis are shown in Fig. 13 while in Fig. 14 a comparison with the human hand is provided.

Using a rapid prototyping process was critical in realizing the biomimetic shapes and features of the hand as well as its complex internal structures that would have been extremely difficult and costly to manufacture by traditional techniques. Moreover, since rapid prototyping allows for a low-cost and fast turnaround from design submission to product visualization, early physical prototypes were developed and tested in order to enhance design parameters and optimize hand performance.

2.6 Tactile Sensors

In order to improve hand control during object grasping and enable sensory feedback to the amputees, commercially available force sensors were customized and integrated in the distal phalanges of the thumb, index and middle finger of the prototype. More specifically, force sensing resistors (FSRs), produced by Interlink Electronics Inc., were selected to be fitted in these fingertips. FSRs are robust polymer thick-film two-wire devices that exhibit decreased resistance when force is applied normal to their surface. They have wide appeal from the standpoint of compact size, low cost, good sensitivity, and simple electronics [51]. Although these sensors are generally appropriate for qualitative rather than precision measurements, their

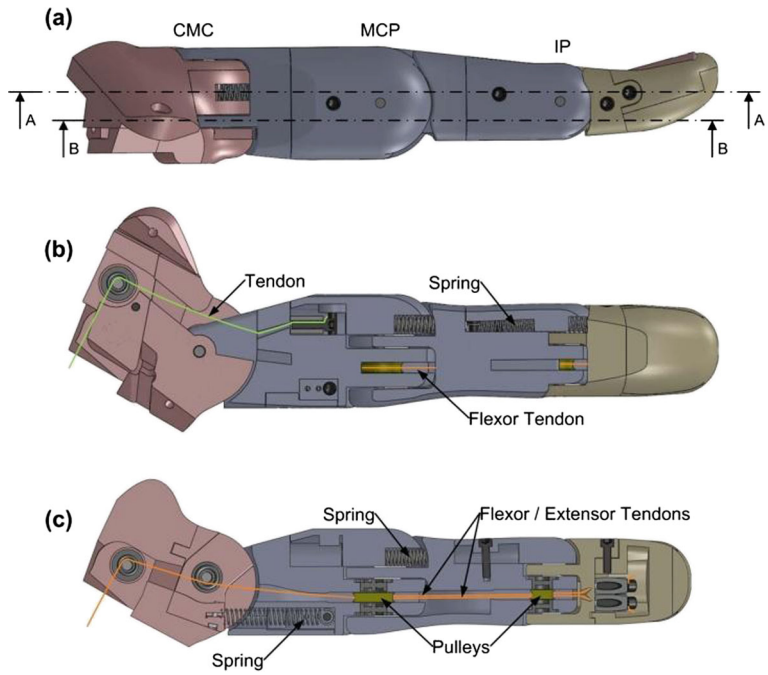

Fig. 12 The designed thumb in **a** top view, **b** cross-sectional A view and **c** cross-sectional B view, showing tendon routing

performance was found to be sufficiently accurate for measuring fingertip forces.

The design and implementation of the distal finger phalanges incorporating FSRs are presented in Figs. 15 and 16, respectively. As it is shown, the smaller off-the-shelf sensor (FSR 400 with an active area of 5.08 mm diameter) was customized and mounted on a printed circuit board (PCB). This PCB was employed to ensure a flat surface underneath the sensor (requisite for proper function) and also to connect with a two-wire cable for interfacing the sensor with its remotely located electronics. This assembly is then covered with a silicone layer to evenly distribute any applied force and improve accuracy and repeatability of the measurements. A similar sensor assembly and structure is also adopted in the distal phalange of

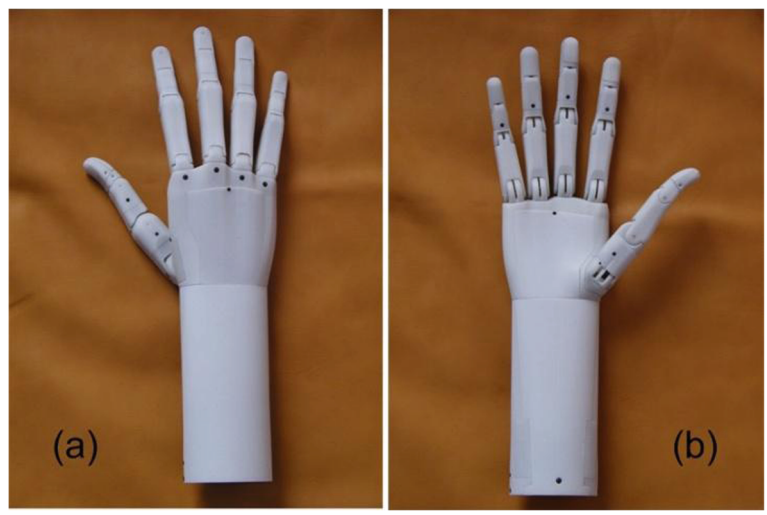

Fig. 13 Prototype of the prosthetic hand in **a** dorsal and **b** palmar view

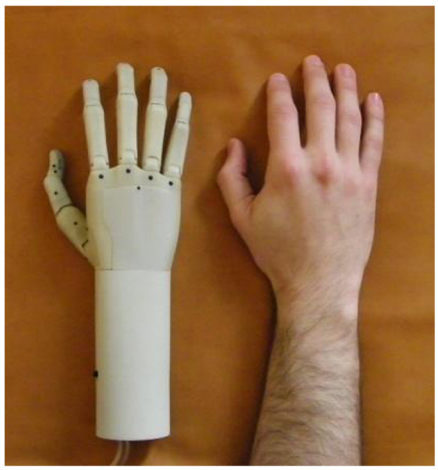

Fig. 14 Comparison between the prosthetic hand prototype and the human hand

the thumb with the only essential difference being the integration of an FSR sensor with larger active area (FSR 402 with an active area of 12.7 mm diameter).

Additionally, the sensory capabilities of the hand were enriched with the integration of a miniature surface-mount thermistor (Panasonic NTC thermistor, Part No. ERTJ1VG103FA) in the distal phalange of the ring finger (Fig. 17). A thermistor is a type of resistor with resistance varying according to its temperature; it was favored over other technologically different temperature sensors due to its quick responses, low cost, small size and easy interface needed for reading its values [52]. Using this sensor, thermosensitivity is introduced in the hand prosthesis allowing for temperature monitoring of the grasped objects and

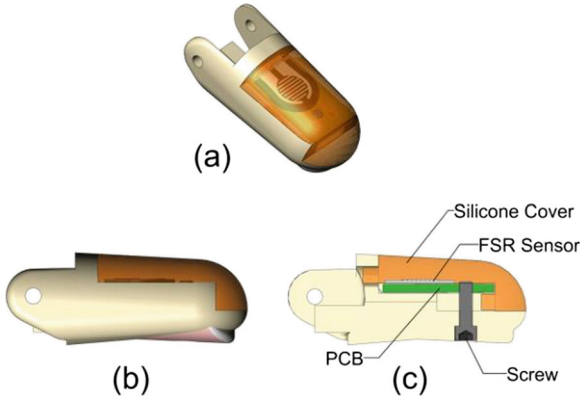

Fig. 15 CAD model of a distal finger phalange incorporating an FSR sensor in: **a** perspective view, **b** side view, and **c** cross-sectional side view

thereby avoiding any damages when touching very hot or cold objects. As in the force sensor assembly, a PCB is employed for the wiring interconnections while a silicone layer is also used for covering the sensor. Silicone is extremely resistant to high temperatures and also reduces heat dispersion and as such contributing towards correct temperature measurements. The effectiveness and responsiveness of the developed sensor assembly was tested and illustrated in Fig. 18. More specifically, at room temperature (32^{o}C), the distal phalange gets in contact with a 50^{o}C hot surface of a thermoelectric module (Multicomp HPE-127-14-06); whenever the temperature change (ΔT) becomes higher than the predefined threshold, a temperature alarm is produced and the phalange is manually moved away from the hot surface. The electronics used for acquiring the sensor measurements are described in Section 3.4.

2.7 Cosmetic Cover

A glove-like cover of 1 mm thickness for the hand prototype was modeled and then molded using a silicone rubber material (Smooth-On Dragon Skin) with shore hardness of 10A (Fig. 19a). This material is durable and resistant enough to puncture or ripping while having high elasticity; hence, when the glove is on, no severe interference with the hand performance (range of motion, speed and force output) occurs. It also has much higher coefficient of friction than the plastic sintered material of the hand chassis resulting in more stable grasps with lower needed contact forces. In addition, the developed glove, when fitted on the hand prototype (Fig. 19b), serves as a protective cover from wear and dust while also providing a more normal anatomical silhouette.

3 Actuation System and Control Electronics

3.1 Actuation Concept

As it is already mentioned in Section 2.2, owing to weight and space restrictions, an underactuated tendon-driven mechanism is implemented in the prosthetic hand design allowing each digit to be independently controlled. Moreover, non-conventional muscle-like SMA actuators, and specifically NiTi actuator wires, are intended to be integrated in the

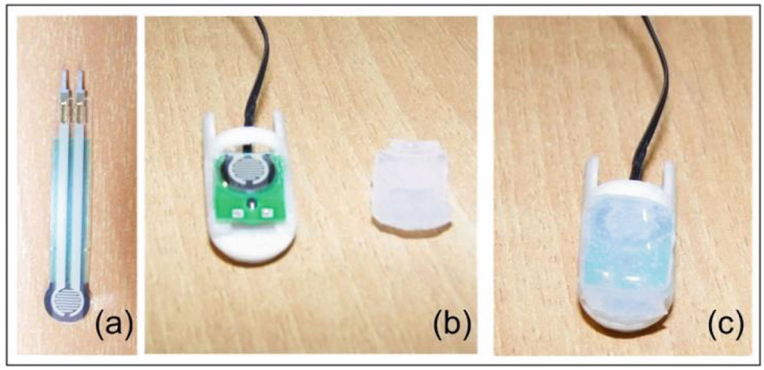

Fig. 16 **a** Interlink Electronics FSR 400 sensor. **b** Distal finger phalange incorporating the FSR 400 sensor, and **c** fully assembled including a silicone cover

hand chassis. These actuators display one of the highest work density at 10 J/cm^3 which is a factor of 25 times greater than the work density of electric motors and is able to lift more than 100 times of its weight [53]. In addition, compared to the whirring DC motors of the current commercial hand prostheses (with an operating noise of about 50 dB [54, 55]), SMA actuators are completely silent. Furthermore, using SMA actuators there is no need for complex and bulky transmission systems which are mostly responsible for the increased manufacturing and assembly cost of the conventionally actuated prosthetic hands.

However, these actuators can only provide force in the powered direction (one-way actuators); hence, for controlling the motion of the active joints of the hand, these actuators must be paired with bias-force mechanisms. These mechanisms can either be implemented using other antagonistic one-way actuators (active opposition), similarly to the opposing muscle pairs of the human hand, or using bias springs (passive opposition). Although, active opposition has the potential benefit of increasing dexterous capability, particularly in regards to speed and small force interactions, it requires doubling the number of actuators,

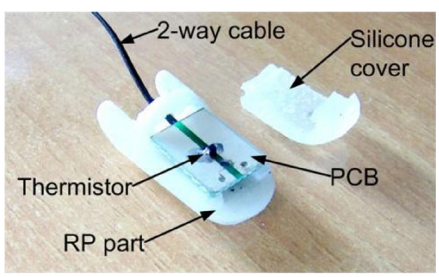

Fig. 17 Assembly of the distal finger phalange with an embedded temperature sensor

exacerbating packaging and weight issues. Therefore passive opposition seems to be a more suitable choice given the design constraints of the presented prosthetic hand system. Taking also into consideration the low energy efficiency of the SMA actuators - under practical settings, efficiency is typically below 5 % [56] - and the absence of any back-lock mechanism that would allow the hand to maintain grip on an object without power being supplied to the actuators, bias coil springs were selected to be opposed to the hand opening. In this way, a powerless adaptive grip is provided. The hand is closed at rest in a fist position and electrical power is required only for hand opening; this results in less power consumption which is a key concern in the battery-operated prosthetics. Similar voluntary opening approaches have already been adopted in some commercial body-powered prosthetic devices [57].

In this research work, one SMA actuator is used for the active extension of each digit as well as thumb adduction, while preloaded coil springs act antagonistically to these movements. The bias springs of the fingers are located inside the palm and forearm area of the hand, whereas, as it is already shown, the bias springs concerning the thumb motion are placed inside its structure in order to facilitate assembly. These springs must be as soft as possible to limit the unnecessary bias forces during hand opening, yet having a high preload force for stable and firm adaptive grasps of the most common objects. Moreover, in case of heavier objects, the prosthetic hand design made provision for the inclusion of three additional SMA actuators providing extra flexion force to the thumb, index and middle finger. Thus, these three actuators along with the six previously ones (five for extension movements of the digits and one for thumb adduction)

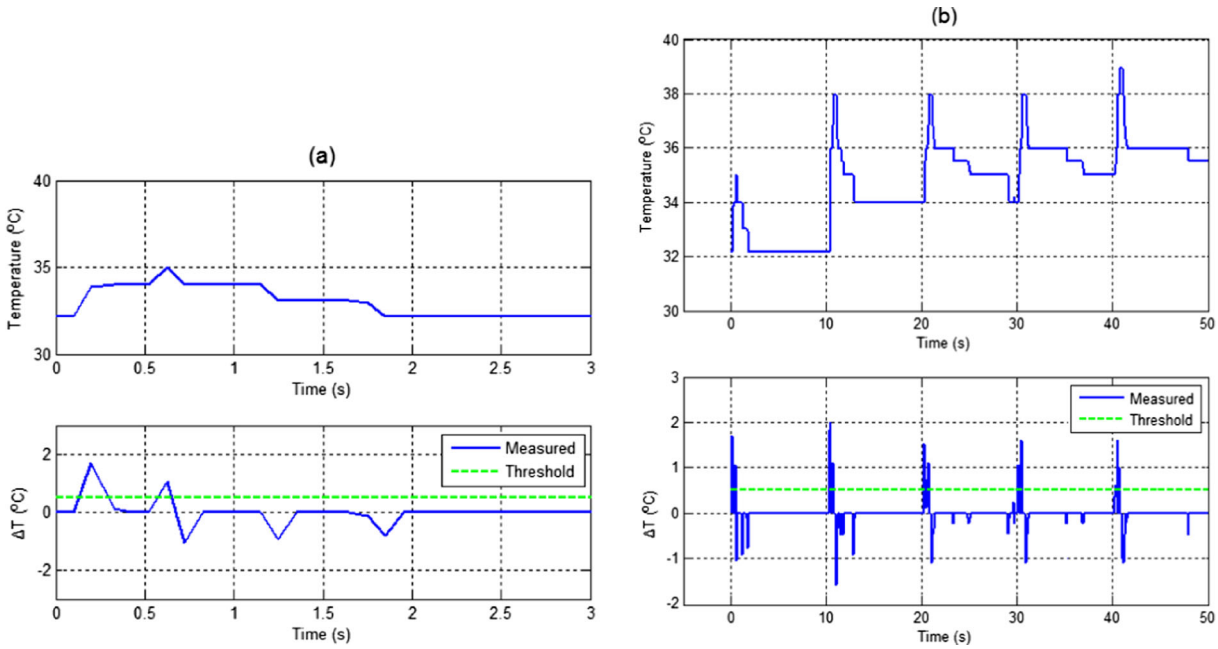

Fig. 18 Response of the temperature sensor assembly in **a** contact with a hot surface, and **b** repeated contact with a hot surface at every 10 seconds

raise to nine the total number of SMA actuators which must be incorporated in the hand chassis.

3.2 Development of SMA Actuation Units

The most practical SMA actuators to use in achieving our research goals were proven to be the specially processed NiTi wires, known as Flexinol and commercially available by Dynalloy Corporation. These wires are low-cost one-way actuators that are optimized to contract in length when heated above a certain transition temperature, exerting significant stresses (maximum safe stress: 172 MPa), and if used properly can last for tens of millions of cycles [58]. Their heating can be achieved using various methods though the most convenient and easily applicable one

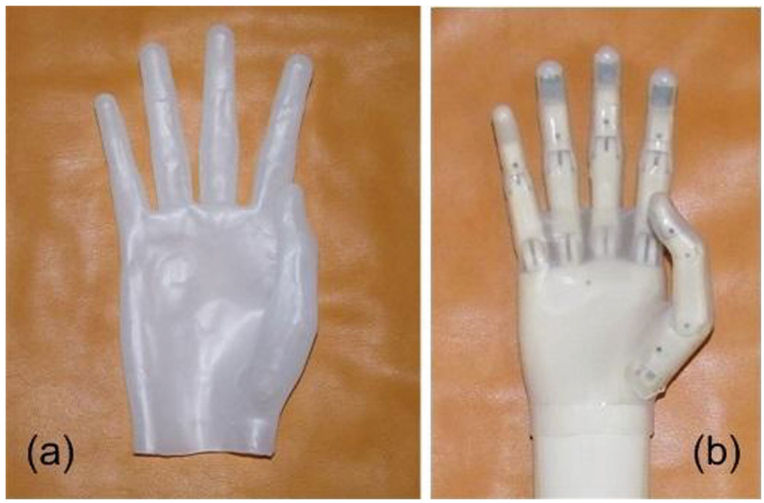

Fig. 19 **a** Custom-fabricated silicone glove. **b** Hand prototype covered by the silicone glove

is the electrical resistance heating: applying a voltage across these wires, they can contract in less than one second. When voltage is turned off, they are allowed to cool and can elongate again by a relatively small bias force. However, since these actuators are thermomechanical in nature, their cooling rates through natural convection are much slower than their heating ones.

There are various methods to improve the speed of cooling such as using forced air, heat sinks, or liquid coolants but the simplest one is using smaller diameter wires. The smaller the diameter the more surface to mass the wires have and the faster they can cool. Though thinner SMA wires are faster, they are also much weaker; in other words, there is a trade-off between speed and force. The loss of force can be recovered by increasing the number of actuators working together. One method is to place multiple actuator wires in parallel as a bundle. However, as it was experimentally shown in [59], bundling can be an inefficient method of combining work outputs of multiple actuators. In case it is only necessary to double the force output, a more practical work-summation method, which is also adopted in this research work, involves the use of only one actuator wire folded in the middle forming two electrically equal pathways.

Another key concern when using these wires as actuators is their low strain capabilities: they can contract only about 3–4 % of their length. Henceforth, long wires are needed to have a fair amount of linear displacement (i.e. stroke). But, taking into consideration the tight dimensions of the hand structure, the length of actuators must be kept as short as possible. MIGA Motor company has already introduced in market such compact actuators with multiple Flexinol wires using a patented displacement multiplication principle [60]. However, their specifications do not comply with the needs of this research. Therefore, other wire layouts were investigated [26] and eventually a N-shaped layout was adopted. This wire layout is also combined with the aforementioned folded pattern for doubling the force output (Fig. 20) and implemented within a compact structure having the SMA wire wrapped around miniature nylon washers (Fig. 21). The smaller washers shown in Fig. 21 are used as structural elements of the actuation unit (AU). In addition, for insulation purposes and faster cooling times, SMA wires are running through narrow-gauge PTFE tubes (Fig. 21, 22). Three PCBs of 0.8 mm thickness were utilized as support structures of

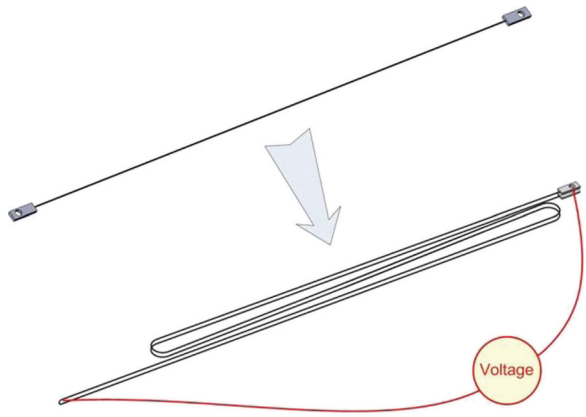

Fig. 20 SMA wire in a N-shaped folded pattern. The two ends of the SMA wire are crimped with custom-made brass eye terminals

the SMA wire layout while bringing the necessary wirings for interfacing with the electronics of the AU. Moreover, brass screws are employed as structural elements. Due to their high conductivity these screws are also used for carrying power and control signals and interfacing with other boards, eliminating in this way the need for a connector and thus keeping the size of the AU as small as possible.

Attaching SMA wires to make both a physical and an electrical connection was done by crimping. SMA wires tend to maintain the same volume, so when they contract along their length, they simultaneously grow in diameter, and thus expanding inside the crimps and holding more firmly as the stress increases through pulling. Custom-made brass eye terminals are used for both ends while at the middle point, where the wire is folded, a brass tube is crimped on. A silver bolt ring is

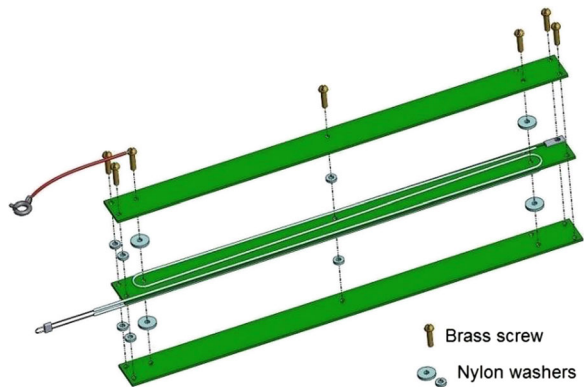

Fig. 21 Exploded view of an SMA actuation unit

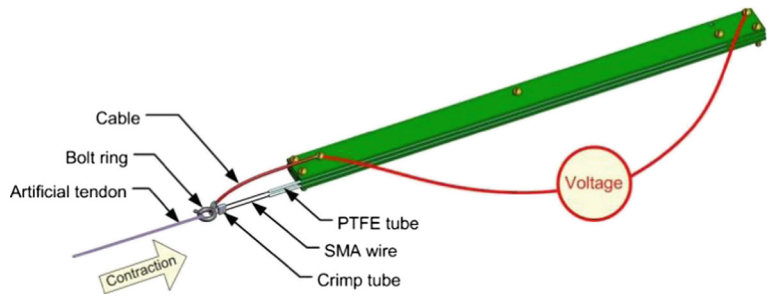

Fig. 22 Operating principle of an SMA actuation unit

used for joining the SMA wire with an artificial tendon at its movable folded point. A flexible copper cable is soldered at its one end on this ring and at the other one on the upper PCB; in this way a parallel electrical circuit is formed. So, when an electrical voltage is applied as shown in Fig. 22, the AU contracts and moves the attached artificial tendon.

Each of these AUs was chosen to consist of a Flexinol wire having a 0.25 mm diameter and a transition temperature of 90 ^{o}C. According to its technical specifications provided from the manufacturer [58], this wire can safely exert forces up to 9 N; hence the AU with its folded pattern is able to produce forces up to 18 N. Its cooling or relaxation time (which refers to the time it takes for the wire to fully return to its cold state by natural convection at 20 °C) is about 4.5 s. As it will be discussed later, only a fraction of the available net stroke of each AU will be used for the hand movements and thereupon better response times are to be expected.

In Fig. 23, one newly developed SMA AU is presented. As it is shown, a small-sized PCB that brings all the necessary electronics for driving an AU was also developed and mounted on its upper surface rendering it completely self-contained. Moreover, considering the limited available space inside the hand prototype, a dual SMA AU was also developed and shown in Fig. 24. This comprises of two SMA wires in the N-shaped folded pattern. Towards this scope, two additional 0.8 mm thick PCBs are employed as support structures and another electronic board is mounted on the upper surface of the AU for driving the second actuator wire. Thus, although the two SMA wires are packed together, they act as completely independent actuators. The specifications of the developed single and dual AUs are summarized in Table 2. The length and width dimensions refer to those of the structural PCBs. In the height measurement, embedded electronics were also taken into account. Regarding the AUs of the thumb, as it will be shown in the next section, shorter length of SMA wires are used in order to fit within the limited available space inside the hand prototype and thus smaller strokes can be achieved.

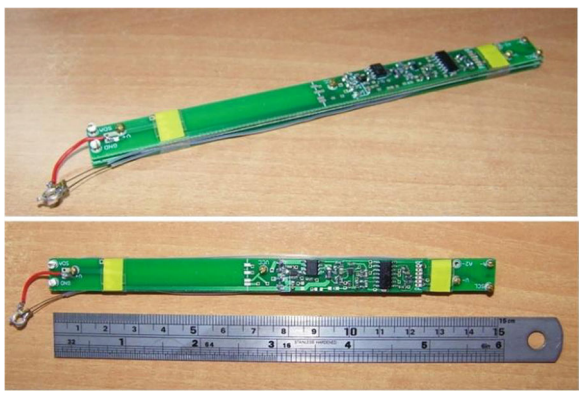

Fig. 23 SMA actuation unit with embedded electronics

3.3 Integration of the Actuation System

Three single SMA AUs and another three dual SMA AUs are mounted on a common PCB, as shown in Fig. 25, by means of the brass screws. This PCB interfaces the AUs with a main control board (MCB) whose components are detailed in the next section. The whole actuation system along with the MCB is integrated in the hand prototype as shown in Fig. 26; the covers are removed to reveal the inner assembly of the hand. The whole design was targeted to facilitate easy access to the AUs allowing for quick maintenance and service.

The four bias springs that keep all the fingers in a closed position when AUs are not activated are also shown in Fig. 26. These are preloaded extension springs originated in the posterior underside of the hand prototype. Their spring preload was selected

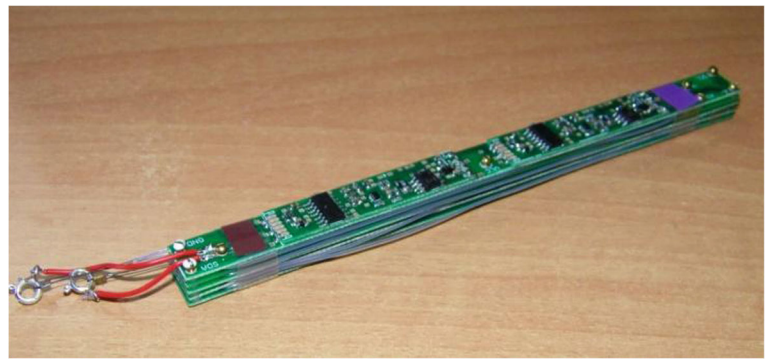

Fig. 24 A dual SMA actuation unit with embedded electronics

to be equal to 6.75 N and when the fingers are fully opened each of these springs exert a flexion force of about 8.75 N - a force magnitude which is much lower than the 18 N of force output of the AUs employed for the antagonistic extension movements of the fingers.

Given these force values, the force/torque capability of a representative finger (index) during flexion is illustrated in Fig. 27. More specifically, the fingertip force and the torques at its two underactuated joints are presented for the trajectory of Fig. 10. As it is shown, fingertip forces of 1.6-3.3 N can be provided due to the preloaded springs, while higher forces of 3.85-11.5 N are also available (excluding the ring and little fingers) by powering the AUs that provide extra flexion force. Given these values, the total combined fingertip force of the four fingers is expected to be between 10.9 N (stretched out position) and 29.6 N (fully closed position). These forces are relatively low compared to the exerted forces at the human fingertips (up to 30 N), yet adequate for accomplishing most of the ADLs [36]. Although SMAs have one of the highest power-to-weight ratio among all the actuators, their low energy efficiency deters any thoughts of employing more Flexinol wires for providing higher forces.

In addition, although compact AUs were developed in order to pack long actuator wires and overcome the low strain issues of the SMAs, the total length of the presented hand (including the small-sized forearm which houses the actuators and electronics) is about 100 mm longer than that of the commercial hand prostheses. Hence, this may hinder the fitting of the proposed device to the amputees with long stumps.

The weight of the fully assembled prosthetic hand, after the integration of its actuation system and electronics, is about 310 grams, and with the silicone glove on the total weight does not exceed 350 grams. So, compared to the current high-tech commercial prosthetic hands that weigh more than 450 grams without their battery (which is usually hosted in the prosthetic socket proximally to the residual limb) [61], the developed hand is far lighter. This is of primary importance among prostheses users; based on recent studies [7, 8], the weight of the prosthesis is still one of the primary reasons of user fatigue and discomfort that lead to its early rejection. Thus, the presented prosthetic device

Table 2 Specifications of the SMA actuation units

Specifications (units)	Single	Dual
Length/Width/Height (mm)	147/10.5/6.5	147/10.5/10
Mass (g)	12	18
Output force/ea. (N)	18	
Stroke/ea. (mm)	15 (12.5 for thumb AUs)	
Peak power/ea. (W)	29 (24 for thumb AUs)	
Bandwidth (Hz)	0.2	
Actuator type	High Temperature (HT) Flexinol Actuator wire of 0.25 mm diameter	

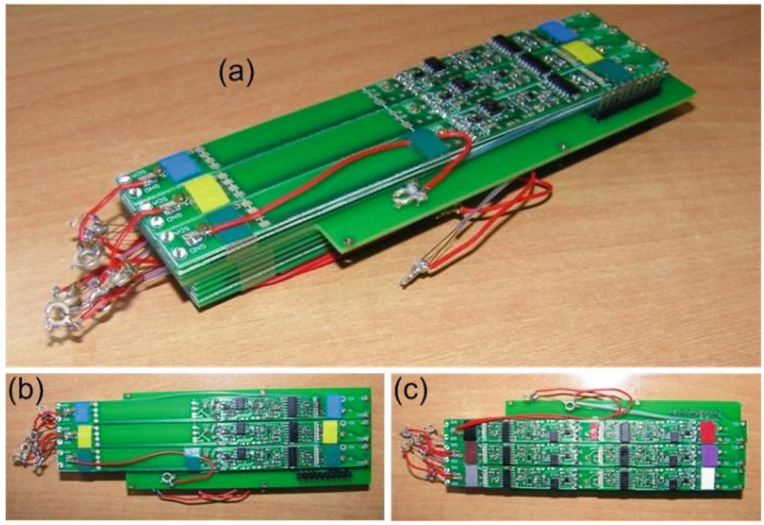

Fig. 25 SMA actuation units mounted on a common PCB in: **a** perspective view, **b** top view, and **c** bottom view

can be more easily accepted as a technical aid by the amputees.

3.4 Control Architecture

A block diagram of the general electronic architecture is illustrated in Fig. 29. Analytically, a host microcontroller (master), integrated in the custom-made MCB (Fig. 28), is connected through a Two Wire Interface (TWI) to nine local microcontrollers (slaves) embedded in the AUs (one per single AU, two per dual AU). These slave microcontrollers are used for driving the corresponding SMA actuators. As it is already mentioned, the actuation is controlled by electrical heating of the SMA wire. Though this could be done using a direct electrical current, Pulse Width Modulation (PWM) method was preferred. In this scheme, a fixed voltage is applied for a percentage of a pre-set

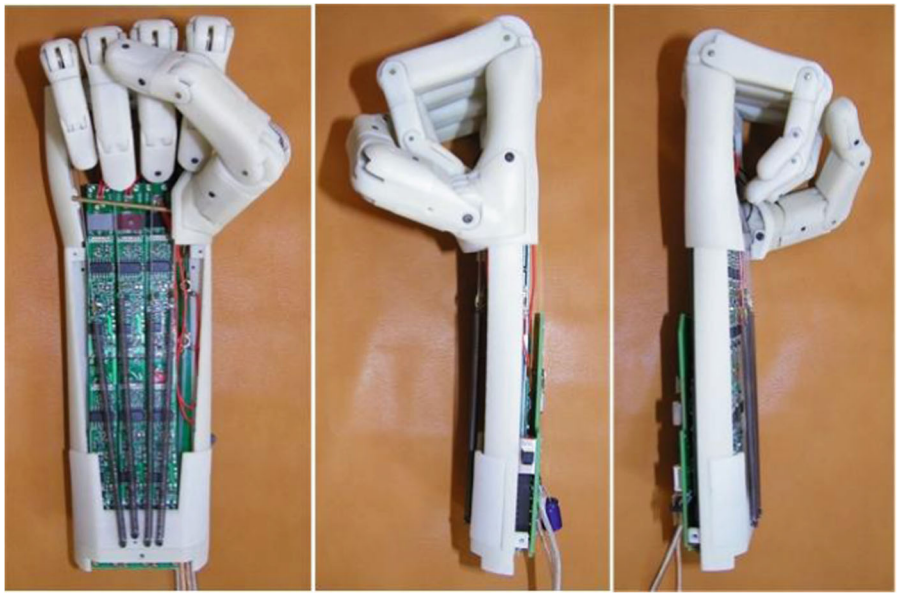

Fig. 26 Hand prototype without its covers integrating the actuation system and electronics

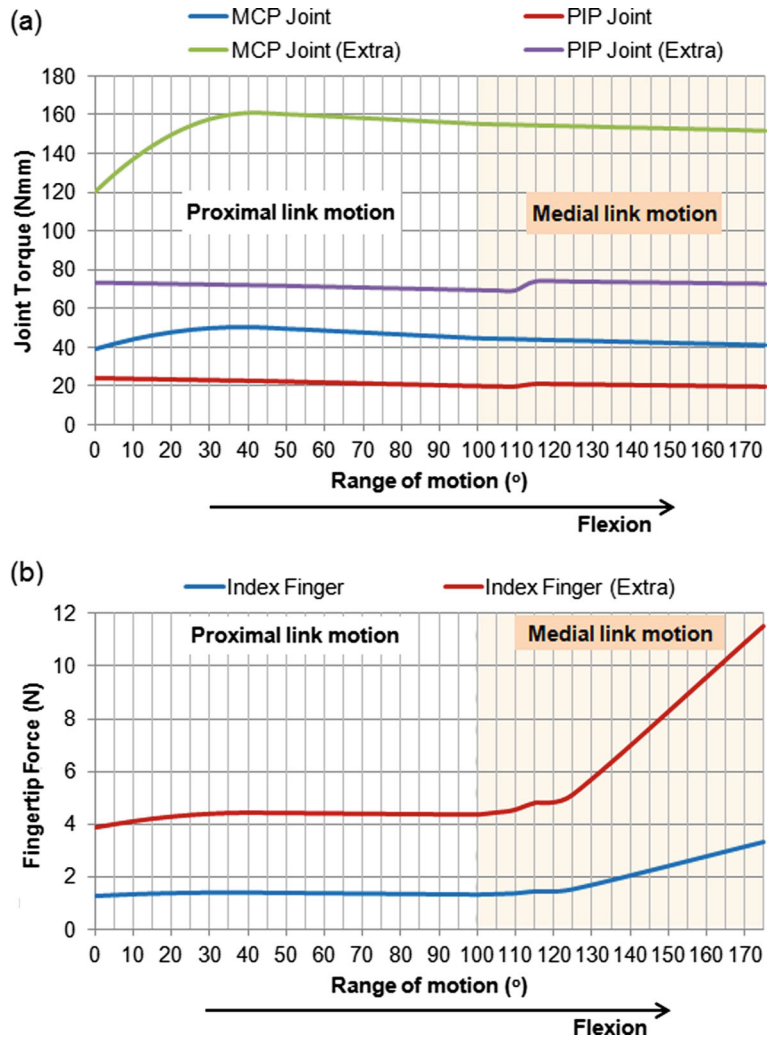

Fig. 27 **a** Joint torques and **b** Fingertip forces of the index finger

period. As the percentage on-time to off-time in a single period (referred to as the duty cycle) is changed, the aggregate amount of power delivered to the SMA wire, and hence its contraction, can be controlled [60]. Moreover, the averaging effect of the on-off voltage durations coupled with the relatively slow response time of the SMA, enables a uniform heating with little generated waste heat, resulting thereby in improved energy efficiency [24]. PWM activation is also popular because of the ease with which it can be implemented using microcontrollers. In our case, each slave microcontroller (Atmel AVR 8-bit: ATtiny44A) generates a PWM signal that controls the gate of a power MOSFET which in turn acts as a switch to modulate the voltage applied to the actuator.

All of the conventional rules for electrical heating apply to the SMA wire, except that its resistance goes down as it is heated and contracts (contrary to the general rule of increased resistance with increased temperature). This characteristic can be used for position feedback of the actuator; in fact, by monitoring its electrical resistance, a good estimation of the contraction level can be obtained [62, 63]. Thereupon, there is no need for additional position sensors which would increase complexity and cost of the design. The electrical resistance is easily calculated by measuring the voltage drop and electrical current flowing in the SMA actuator. This is achieved by means of the analog input pins and in-built 10-bit multichannel analog-to-digital (A/D) converter of each slave microcontroller.

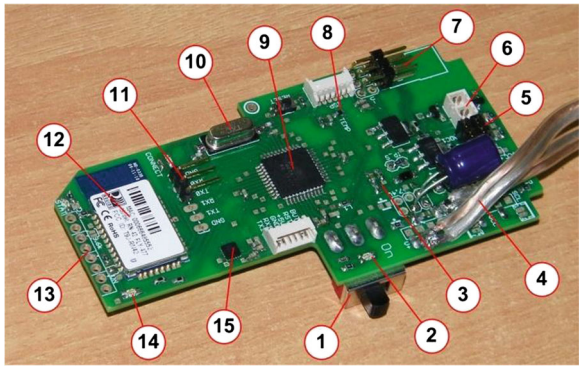

Fig. 28 Main control board (MCB) including: **1** on/off switch, **2** bicolor status LED, **3** voltage supply sensor, **4** power supply cables, **5** connectors for FSRs (control interface), **6** connectors for tactors, **7** pin header for servomotors, **8** temperature sensor, **9** microcontroller, **10** external quartz crystal, **11** pin header for UART transmission, **12** Bluetooth module, **13** vias for connecting the wirings of the fingertip sensors using press-fit pins, **14** bicolor LED for visual feedback, **15** triple-axis accelerometer

One surface mount thermistor is also embedded on each of the electronic boards of the AUs and interfaced with an analog input of the corresponding slave microcontroller. Although the provided temperature measurements do not reflect the actual temperature values of the SMA wires, these sensors are very useful for overheating protection and control improvement of the AUs.

Besides the TWI communication with the SMA drivers, the master microcontroller (Atmel AVR 8-bit: ATmega164A) is interfaced with a high number of sensors through its analog inputs. More specifically, 10-bit samples, with a sampling frequency of 1.2 KHz, are taken from: a) the four fingertip tactile sensors (three FSRs and one thermistor), b) two additional FSRs that can be used for hand control by the amputees, c) a thermistor that measures the ambient temperature of the MCB, and d) a supply voltage sensing configuration. It is noted that only one supply voltage source is used for powering the developed hand and its actuators (this voltage is the one used for PWM driving of the actuators). Wherever lower voltage amplitudes are needed (e.g. for the operation of the microcontrollers), these are generated by voltage regulators incorporated in the MCB. Moreover, a triple-axis 10-bit accelerometer, connected via TWI to the master microcontroller, is also included in MCB, providing shock monitoring as well as motion and orientation detection of the hand apparatus.

The MCB is also equipped with the necessary electronics for driving two vibrotactile feedback devices (vibration motors known as tactors). These devices – usually placed on the remnant limb with an elastic cuff – can convey information to the user in case visual feedback is inefficient or unnecessary [64]. For example, they can be used for force feedback varying their degree of vibration according to the signal strength of the FSRs of the fingertips. Based on initial experiments, the delay between the force perception and the generation of the vibration feedback was measured and found to be 0.3 s. This time is fast enough allowing for a timely user reaction in order to avoid object breaking. However, this type of feedback stimulus, though easily perceived by the users, causes a little unpleasantness [65].

Additionally, a high-brightness bicolor (red/green) LED is embedded on the MCB and is driven using PWM signals generated by the master microcontroller. This visual feedback type can be used complementary or alternatively to the vibrotactile feedback [66].

Moreover, the MCB includes hardware for driving two servomotors which can be used for various hand motions, e.g. forearm rotation. To this direction, a proof-of-concept structure which includes a servomotor and can be mounted at the base of the proposed prosthetic hand was developed and successfully tested (Fig. 30).

The master microcontroller is able to communicate with a personal computer (PC) either serially via a UART protocol or wirelessly over short distances using a Bluetooth module. For the supervision and control of the prosthetic hand system, a graphical user interface (GUI) was developed in LabVIEW environment. Within the context of this paper, experimentation is done manually through this GUI, though, as illustrated in Fig. 29, other three methods of hand control were also implemented via: a) a dataglove that captures the natural hand movements, b) electromyographic (EMG) signals acquired from two surface electrodes on upper limb muscles [67], c) two FSR sensors as described in [68]. Having the FSR sensors interfaced directly to the master microcontroller enables the future implementation of real-time FSR control to the microcontroller level and thus obviating the need for a PC. On the contrary, in EMG control, a PC is requisite for acquiring and analyzing the surface EMG data (using a Delsys Bagnoli – 2 EMG system, and a National Instruments USB-6009 data acquisition

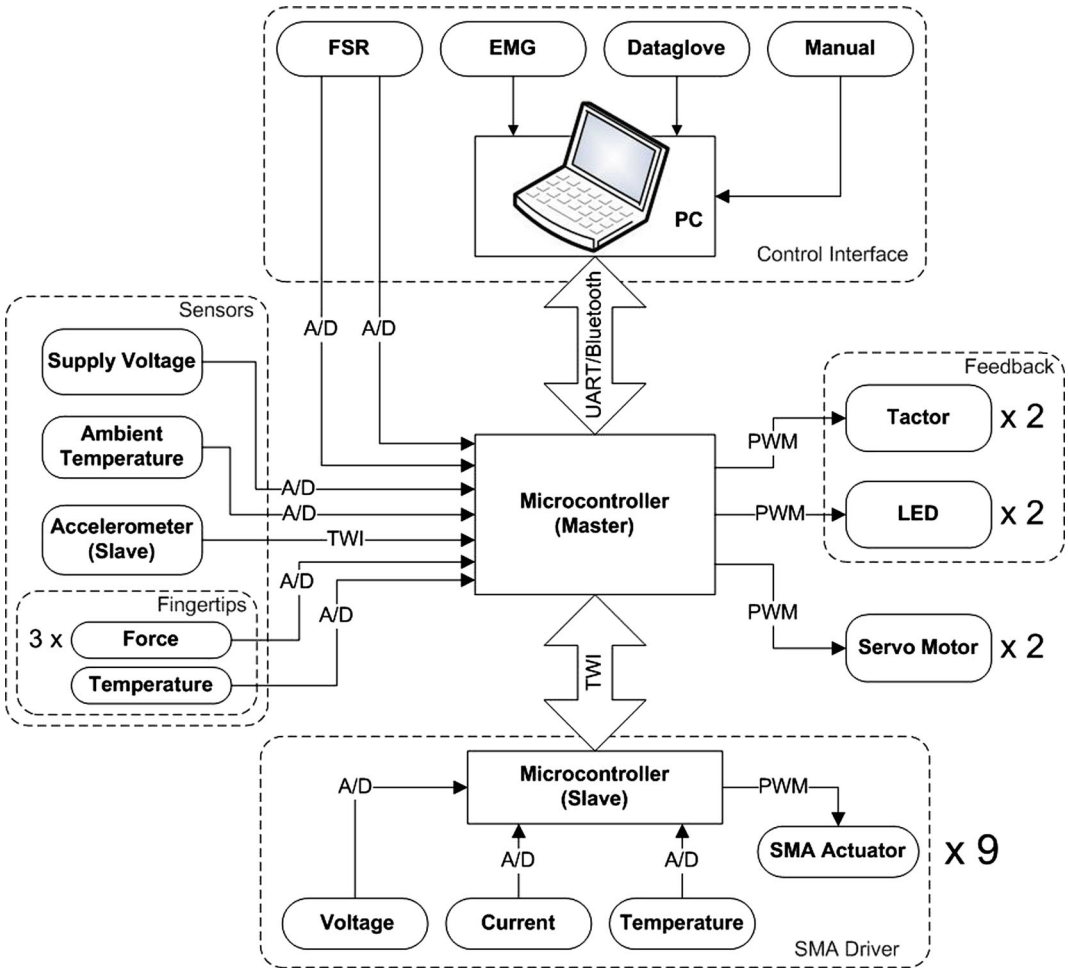

Fig. 29 Block diagram of electronics and communication

device); in the future, the electronics needed for real-time EMG control are planned to be also integrated in the MCB (their weight contribution is expected to be less than 5 grams).

In manual control, the PC is in charge only for sending the control references to the master microcontroller. Then the master microcontroller carries out the overall hand control apart from the part that concerns

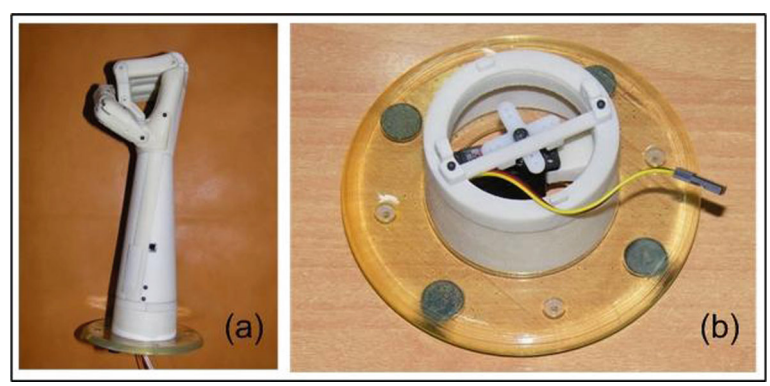

Fig. 30 **a** Hand assembly including a forearm rotation structure. **b** Close-up view of the forearm rotation structure incorporating a servomotor

the control of the SMA AUs which is implemented in the slave microcontrollers.

4 Experiments and Performance Evaluation

4.1 Open-Loop Experiments

Prior to experiments with the hand prototype, the performance of an SMA AU is evaluated initially using the experimental setup of Fig. 31. As it is shown, an extension spring acts antagonistically to the motion of an AU while a linear potentiometer (Alpha 3SP/S6040N B10K) is used for measuring the displacement level. The selected spring has the same characteristics and preload with the springs cited earlier utilized for passive flexion of the fingers. If needed the spring preload can be easily adjusted by changing the position of its one end and fixing it with a screw on a perforated metal sheet.

The custom-made electronics along with a 13.5 V external power supply are used for driving the AU. The linear potentiometer is also interfaced with these electronics having its voltage output electrically connected to an analog input pin of the master microcontroller. The overall experimentation with the AU is carried out through a GUI designed in LabVIEW. In order to assess speed performance, a pulse voltage input was applied to the AU till the maximum displacement level is achieved. The resulting position response is illustrated in Fig. 32. As it is shown, it takes about 1 s (rise time) for the full contraction (about 15 mm displacement) of the AU and about 4 s (fall time) for its return to the initial position. Thus, for a full actuation cycle, at least 5 s are needed – i.e. an actuation bandwidth of 0.2 Hz can be optimally achieved.

Aiming at a self-sensing position feedback control, the relationship between the electrical resistance and displacement of the SMA AU is also examined and confirmed in Fig. 33. Since the electrical resistance is calculated using the voltage and current measurements, this relationship can only be plotted for the heating/contraction phase of the AU when power is on. As it is illustrated in Fig. 33, initially, the electrical resistance increases without a significant actuator motion and then changes direction and starts to decrease (up to about 15 %) almost linearly with the displacement.

Next, an AU is employed for driving a newly developed finger as shown in Fig. 34. This single-finger evaluation testbed adopts the already described operating principle: when the AU is electrically powered, finger extends (stretched out position), while as soon as power is removed, extension spring acts antagonistically to the AU and flexes back the finger to its resting (closed) position.

Based on the previous experimental results, it becomes apparent that for driving this finger, it would be preferable to exploit only a fraction of the actuation cycle of the AU, and better yet, only the linear portion of its resistance-displacement curve. In this way, improved speed and control characteristics can be obtained. Towards this scope, it was selected to have the extensor tendon of the finger slack at its resting position. Thereupon, when power is applied, the finger is not moved from the very beginning of the actuator contraction; as a consequence, there is a slight delay in the extension time of the finger when the AU contracts, but a significant improvement in the time needed for the finger to return to its resting position when power is off. Moreover, the potentiometer value is rescaled in a way to reflect the displacement level of the extensor tendon and not that of the AU (i.e. 0

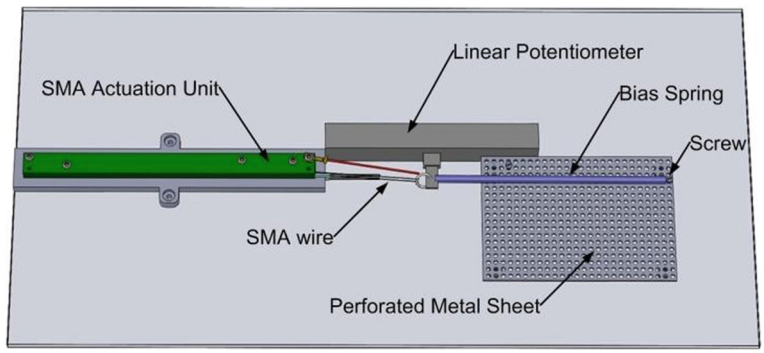

Fig. 31 Experimental setup for an SMA actuation unit

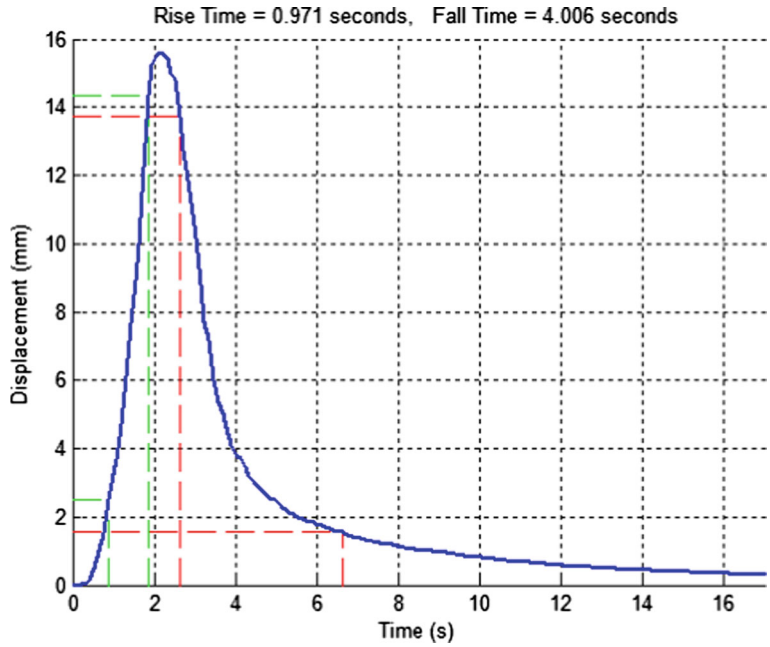

Fig. 32 Position response of an SMA actuation unit to a pulse reference voltage input

mm when the finger is fully closed and 11 mm if fully opened).

Using a pulse voltage input as before, the response of the SMA actuated finger during its extension phase is obtained (Fig. 35). As it is shown, electrical power is removed from the AU when the reference value of its electrical resistance is reached. The choice of this reference value was done considering the fact that the finger continues to extend for some time after the power is off.

In Fig. 36, the resistance-displacement curve for the SMA actuated finger is illustrated. Due to the slackening of the extensor tendon, the nonlinear portion of the AU response (shown in Fig. 33) is not present in finger response. In fact, this curve can be approximately modeled using only linear equations and hence

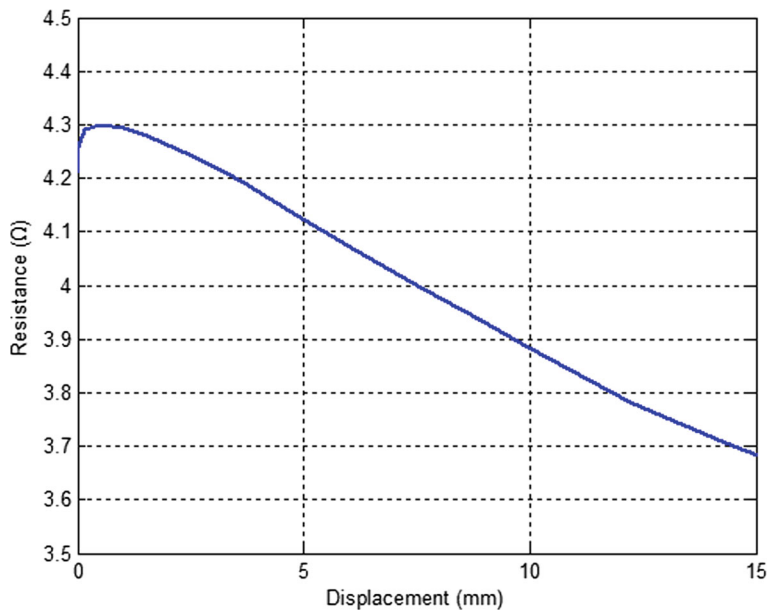

Fig. 33 Resistance-displacement curve of an electrically powered SMA actuation unit

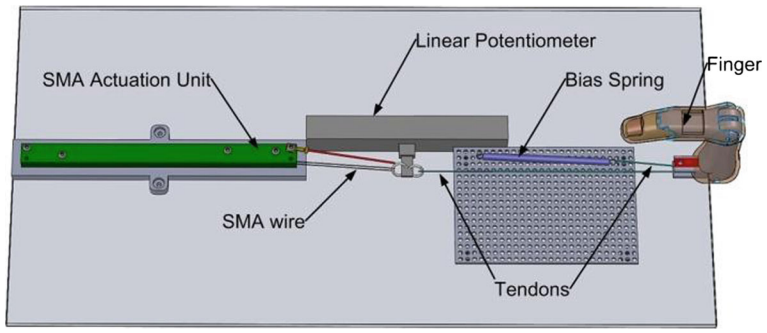

Fig. 34 Single-finger testbed

a position feedback control scheme based on the resistance values can be easily implemented in the slave microcontrollers.

In Fig. 35, the current consumption is also plotted against time. The evident current increase is justified given the decrease of the electrical resistance (as the

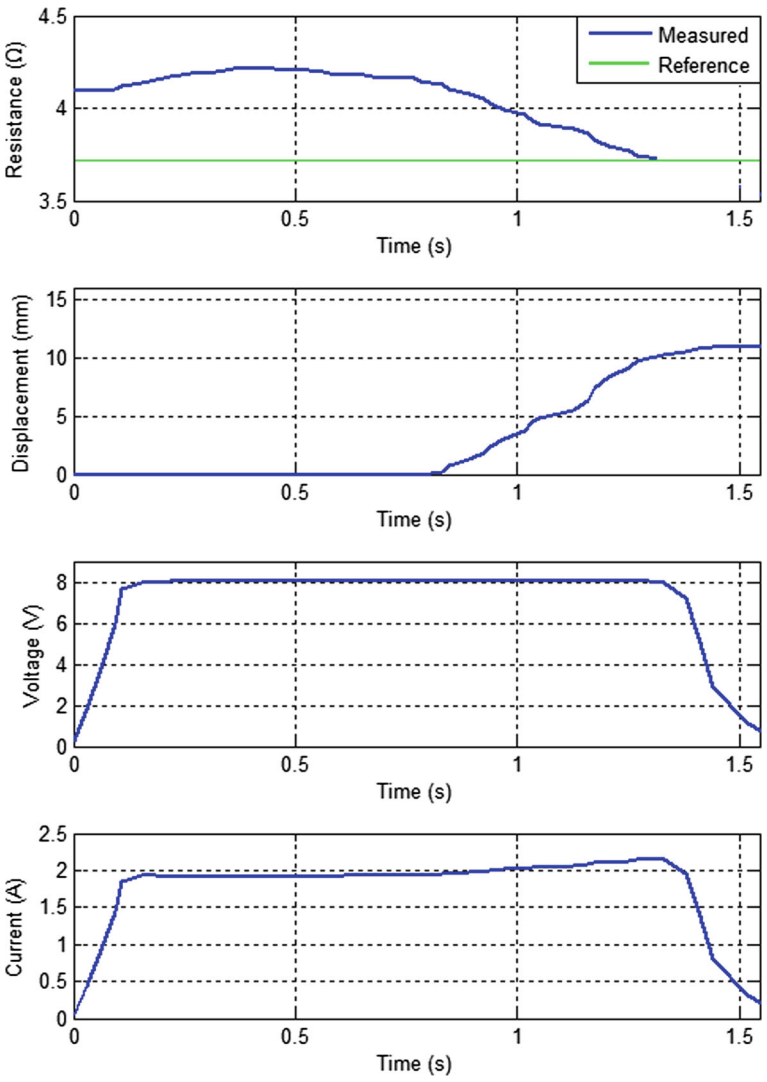

Fig. 35 Response of an SMA actuated finger to a pulse voltage input

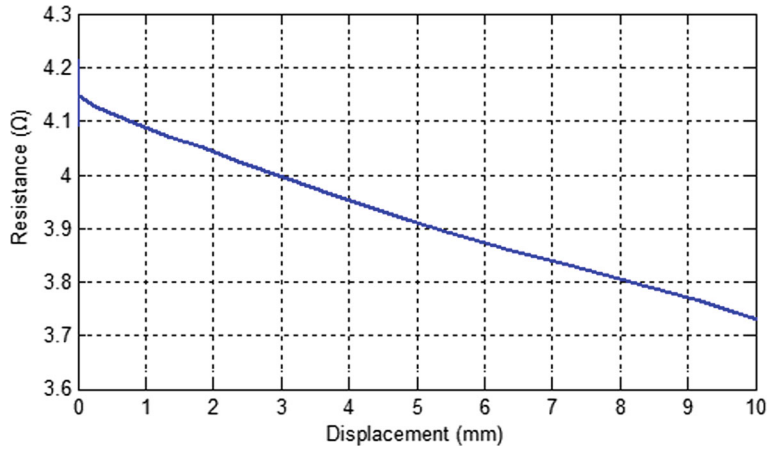

Fig. 36 Resistance-displacement curve for an SMA actuated finger

AU contracts) and the fixed pulse voltage input. The presented voltage and current measurements concern the average values of the PWM signal used in driving the AU. Based on these current measurements, the average power consumption of the AU can be calculated as follows.

Assuming that the PWM signal has a voltage amplitude (peak value) Vs and a duty cycle D and that it is applied across a resistance R, then the average voltage value V_A and root-mean-square value V_{rms} of this signal can be found using the following well-known expressions:

$$V_A = V_S D \tag{1}$$

$$V_{rms} = V_s \sqrt{D} \tag{2}$$

From the Eqs. 1 and 2, the average power P dissipated by the electrical resistance R is calculated:

$$P = \frac{V_{rms}^2}{R} \underset{(2)}{\overset{(1)}{\Rightarrow}} P = \frac{V_A}{R} V_S \Rightarrow P = I_A V_S \tag{3}$$

In our case, Vs is equal to the provided supply voltage (which is also measured by the MCB), hence V_s $=13.5$ V, and the maximum current value, as shown in Fig. 36, equals to I_A $=2.15$ A. Thus, the maximum electrical power consumption of the AU is about 29 Watts (this value along with the one concerning a thumb AU is cited in Table 2). It is noted that this high amount of power consumption concerns only

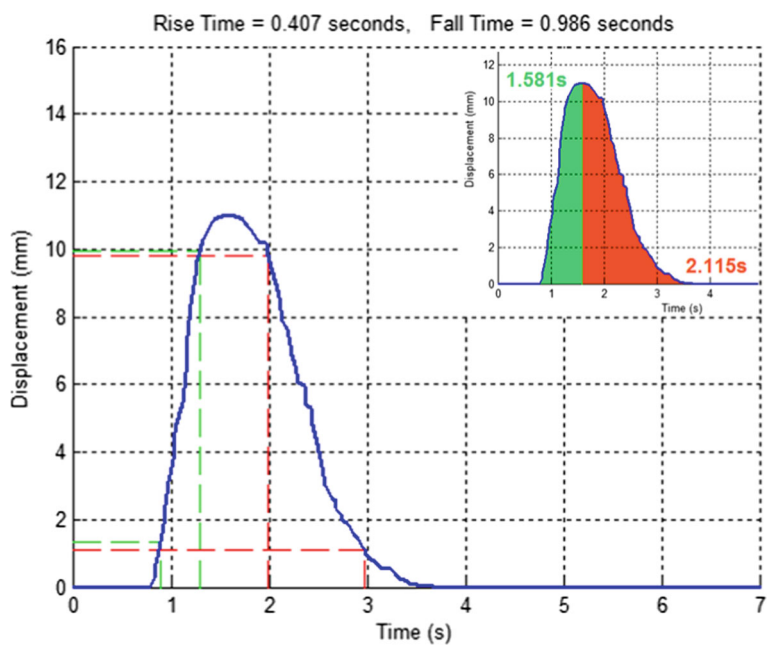

Fig. 37 Position response of an SMA actuated finger to a pulse voltage input

the phase till the desired position is achieved; then, as it will be discussed in the following section, significantly less power is used for maintaining the finger posture.

The position response of the finger during its full actuation cycle is shown in Fig. 37. In the same plot, the response times are also indicated. More specifically, the rise and fall times are about 0.4 and 1 s, respectively, while the times for a full extension and flexion of the finger (ROM: 175°) are about 1.6 and 2.1 s, respectively. Thus, each finger moves at a sufficient speed comparable to the one found in the commercial high-tech prosthetic hands when these are performing typical ADLs [61].

4.2 Position Control of An SMA Actuated Finger

In this section, based on the previously described and modeled relationship between resistance and displacement, a position feedback control scheme is designed and evaluated in the single-finger testbed. The same control scheme will then be implemented in all the slave microcontrollers of the prosthetic hand for position control of the digits.

In literature, various control strategies have been developed to cope with the nonlinearities and hysteresis phenomena of the SMAs. A thorough review of these strategies can be found in [69–71]. In brief, researchers have explored linear controllers as well as nonlinear control schemes including fuzzy logic, neural networks, feedback linearization, optimal control and variable structure control. However, the large range of factors affecting SMA behavior (e.g ambient settings, stress, strain and material fatigue) hinder the robustness of the majority of controllers. As it is underlined in [72], due to the bi-stable nature of the SMA's phase transition (from martensite to austenite form), an on-off type actuation is more suitable than a proportional control. Based on this consideration, various control schemes were devised and evaluated in our testbed before concluding to the following one which proved to be the most effective This novel resistance feedback control scheme combines an on-off control approach with a time-dependent function for resolving heat propagation issues.

So, for a reference resistance value R_{ref}, the applied control voltage V_A to the AU is given in Volts by the following expression:

$$V_A = \begin{cases} V_{on} = f(R_{ref}, H) = a_1 R_{ref} + b_1 H + c_1 \ , R > R_{ref} \\ \\ V_{stay} = f(R_{ref}, H, t) = (a_2 R_{ref} + b_2 H + c_2)t \ + \ a_3 R_{ref} + b_3 H + c_3 \ , \qquad R \leq R_{ref} \end{cases}$$

where R is the calculated resistance of the AU in Ohms, H denotes the measured temperature of the AU in degrees of Celsius, t denotes time in seconds, and the empirically selected coefficients: $a_1 = -3.4$, $b_1 = -0.03$, $c_1 = 21.2, a_2 = -26 \cdot 10^{-3}, b_2 = -3.5 \cdot 10^{-4}, c_2 = 84.6 \cdot 10^{-3}, a_3 = -0.57$, $b_3 = -5 \cdot 10^{-3}, c_3 = 5$.

Next, experimental results of this control scheme are presented for the single-finger setup. Since electrical resistance can only be calculated when power is on, the finger can only be controlled during its extension movements. For carrying out the most common ADLs, two different controllable finger positions are basically needed: a fully extended position and an intermediate one. Therefore, the presented controller is tuned empirically for optimal performance and robustness in these two different positions.

In Fig. 38, the finger response is presented for the fully extended control position. Initially, a high V_{on} signal is generated to quickly contract the AU up to this position (rise time about 0.4 s) and then a V_{stay} signal maintains this position for a short time duration (about 6 s – sufficient time for performing most of the ADLs). Then, the cooling phase of the AU takes place having a fall time of about 3 s. Obviously, if V_{stay} was applied for a shorter time duration, then as previously shown in Fig. 37, the fall time would be much faster. This time deterioration could have been avoided if the actual internal temperature of the SMA wire was measured and used for precise control of its heating rate; however, this method would be impractical in this research work and was therefore not implemented.

As it was previously mathematically described, the amplitude of the V_{on} signal is determined by the R_{ref} value and the temperature H of the AU – for higher R_{ref} (which corresponds to lower reference displacement value) and/or lower H, lower voltage amplitudes

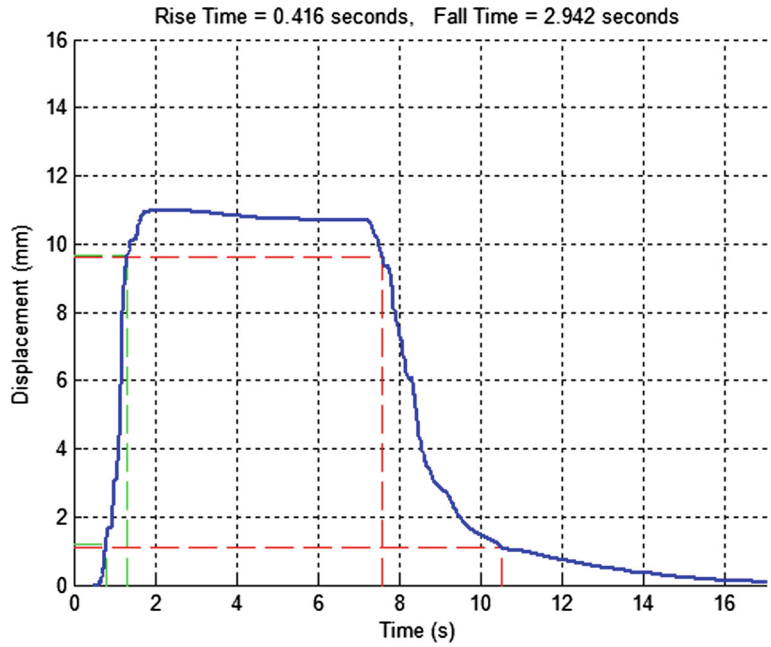

Fig. 38 Position response of an SMA actuated finger for a fully extended reference posture

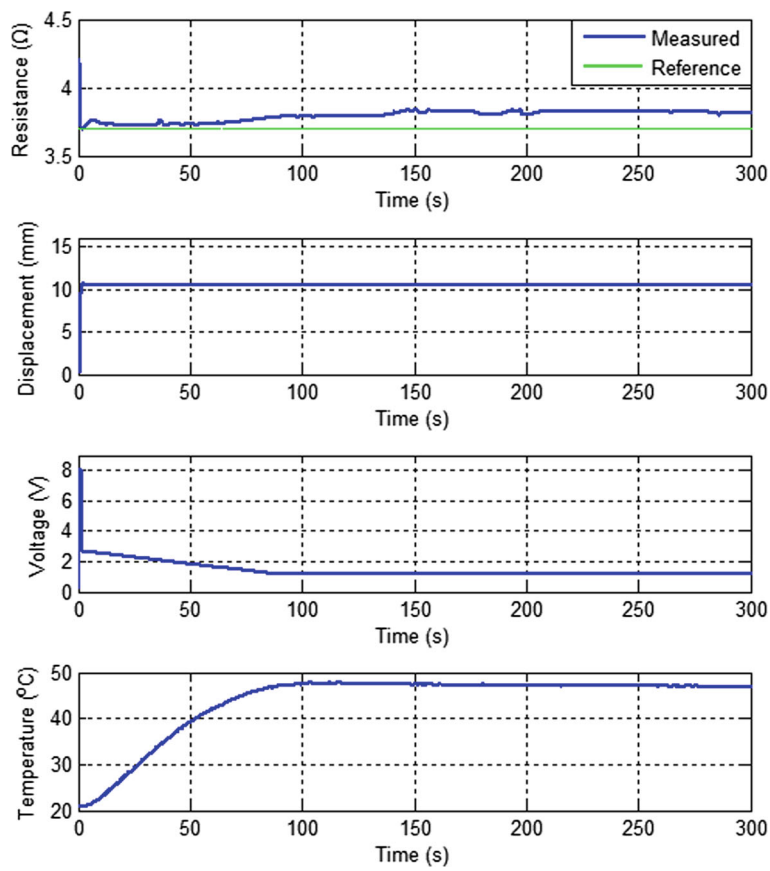

Fig. 39 Position control of an SMA actuated finger for a fully extended reference posture over a time period of 300 s

are needed. The V_{stay} signal depends, in addition, on time and more specifically decreases with time in order to prevent overheating. In Figs. 39 and 40, all these become more apparent, wherein voltage, temperature and resistance profiles are also provided for position control experiments.

Specifically, in Fig. 39, the developed controller is evaluated again in tracking of the fully extended finger position but now for an extended time period of 300 s. As it is shown in the displacement plot, the finger is stabilized in the desired position during all this time period without any noticeable fluctuations - this means that equilibrium between the rate of heating and the rate of cooling is achieved.

The shown reference resistance value R_{ref} concerns only the part of the finger control till the target position is reached. Then the applied voltage is automatically reduced to a much lower value (from a $V_{on} = 8\ V$ to a $V_{stay} < 2.8\ V$), and thus, significantly less power is used for maintaining the finger posture. Due to electronics limitations, the electrical resistance values appear to be less accurate for these lower voltage amplitudes; this was also the cause for not including the measured electrical resistance values in the control function of V_{stay}. However, in the future, more accurate A/D converters are planned to be integrated in the electronics design and better resistance measurements shall be expected even for very small flowing currents, resulting in a significant improvement of the controller.

In Fig. 40, the position response for an intermediate reference posture of the controlled finger (extensor tendon displacement of 7.5 mm) is also provided. As it is illustrated, the finger shows the same good stability performance as in the stretched out position for both short and long time periods.

Overall, the experimental results show the efficacy of the devised control scheme. In the following section, this resistance feedback controller is used for driving safely each digit to a desired position in order the prosthetic hand to perform a certain grip.

4.3 Grasp Experiments

The presented hand prototype is designed to form all the basic types of grasp (the terms grasp, grip, and prehension are interchangeably used throughout this paper), as these are defined in [73], for carrying out most of the typical ADLs. These include the cylindrical grip, spherical grip, tip pinch, and lateral grip.

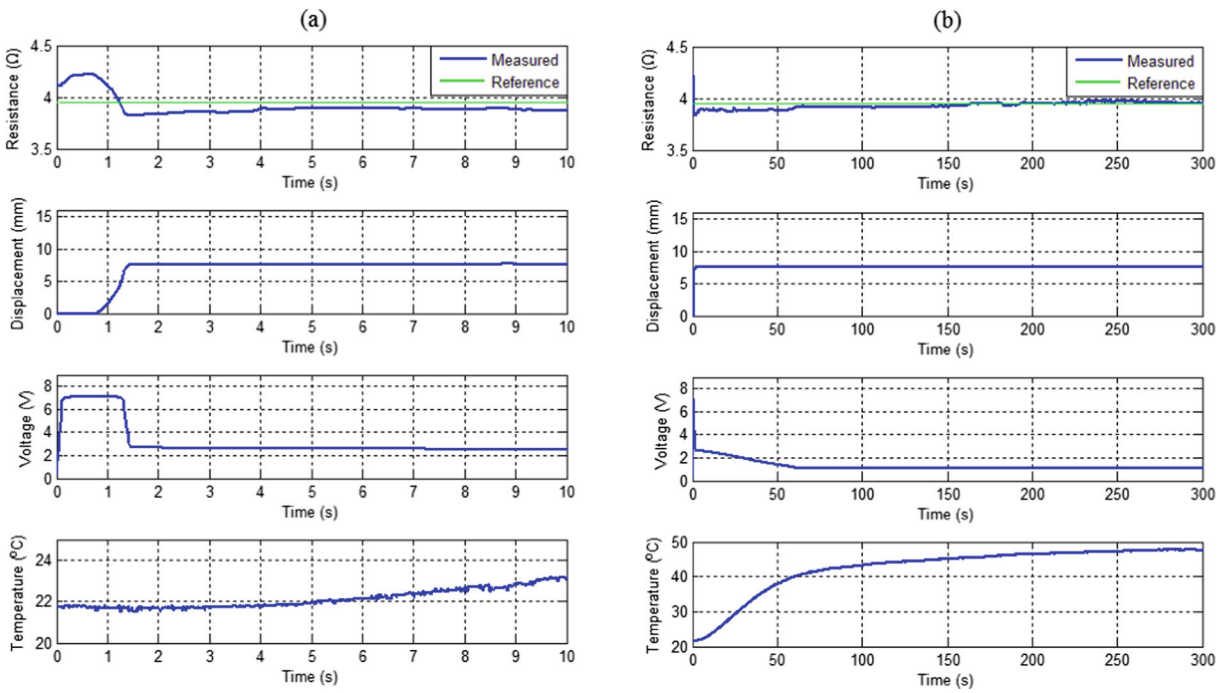

Fig. 40 Position control of an SMA actuated finger for an intermediate reference posture over a time period of **a** 10 s and **b** 300 s

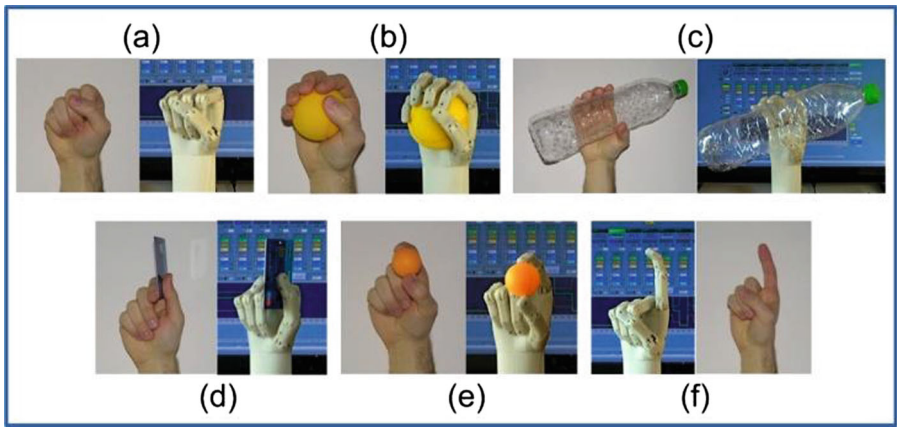

Fig. 41 Comparison between the artificial hand and the human hand in the most common postures and grip patterns: **a** resting posture (fist), **b** spherical grip, **c** cylindrical grip, **d** lateral grip, **e** precision grip, and **f** pointing posture

Note that, in literature, several different taxonomies of the grip patterns exist (a comprehensive overview of these taxonomies can be found in [40]). So, the cylindrical and spherical grips are also commonly addressed as power grips, and the tip pinch as precision grip. According to [11], power, precision and lateral grips are used in 35 %, 30 % and 20 % of ADLs, respectively. A power grip has the thumb opposed to the palm, and it is used when an object needs to be forcefully held. In a precision grip, thumb works in opposition with the index finger mainly to grasp small objects. In a lateral grip, the thumb holds an object against the side of the index finger as in the case when using a key.

In Fig. 41, the developed hand is demonstrated performing the aforementioned common prehension patterns with everyday objects. Besides these patterns, common postures are also demonstrated such as the resting position and index pointing. This pointing posture is very useful in executing common tasks such as pressing buttons or typing on a keyboard. Moreover, in the same figure, each of these postures and grip patterns are juxtaposed with the corresponding ones performed by a human hand, revealing a high degree of resemblance.

All these hand formations are programmed in the master microcontroller and their selection is done manually through the developed GUI. In order to achieve a certain grip or posture, the hand control follows the state diagram shown in Fig. 42. Initially, if the hand is in its resting position ("Neutral") and a signal is triggered ("Go To Position") by a user, the hand starts to form the proper pre-shaping posture in order to perform a certain grip. When this posture is achieved ("Position"), another signal ("Grip") is employed for object grasping. If a higher grip force is needed then another signal ("High-Force Grip") puts the hand in the "Hold High-Force Grip" state.

Each of these states and signals of Fig. 42 corresponds to a different actuator state vector (this contains the control voltage levels - *0,* V_{on}, V_{stay}- of all the AUs). For example, in the case of a power grip selection, in the transient "Go To Position" state, all the AUs that control the extension of the digits are fully powered (V_{on}), while in the "Position" state, the applied voltages are automatically adjusted to their

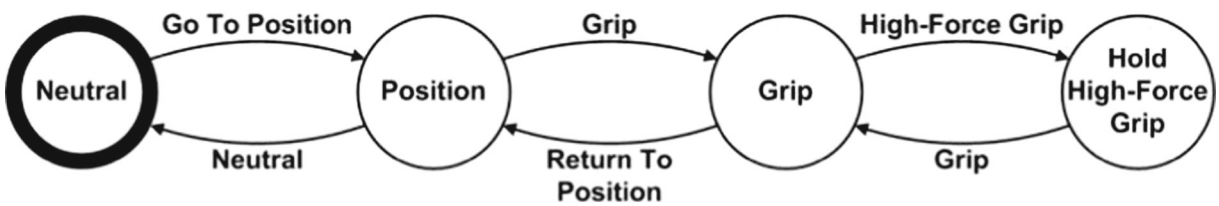

Fig. 42 Control state diagram of the prosthetic hand

V_{stay} level for maintaining a stretched out posture for all the digits. After this pre-grasp phase, the hand is free to grasp an object by powering off all its actuators ("Grip") to allow its fingers to passively adapt to the object geometry or if needed to grasp with higher force by powering the three AUs designated for extra flexion force of the thumb, index and middle finger.

In order to evaluate the grasping capabilities of the hand prototype, experiments with various objects are conducted. In Fig. 43, the hand is demonstrated in pre-shaping and executing the three most common grip patterns (power, precision and lateral). The hand performance in these grips is better illustrated in the accompanied video (Online Resource 1). As it is shown, the prosthetic hand is able to perform stable grasps of various objects with different geometries. The low passive flexion force provided from the bias springs is successfully employed for grasping these objects without breaking them. Besides these results, the prosthetic hand is also tested in grasps of heavier loads; as it was observed, having the silicone glove fitted and within particular friction and geometric conditions, the developed hand is able to stably grasp up to about 1.5 kg cylindrical objects. However, further tests are necessary to determine the actual hand performance in such high-force grips. In any case, compared to the commercial multi-DOF prosthetic hands, the grasping force of the developed hand is low (e.g. the latest release of the i-Limb hand can provide power grip forces of more than 10 kg [10]), yet sufficient to perform most of the ADLs [36].

Based on the grasp experiments conducted so far, the performance of the developed AUs has not been compromised even though they have already been tested for thousands of actuation cycles. Considering the strain and stress conditions of the presented application as well as the provided specifications of these actuator wires [58], it is expected that even after hundreds of thousands of cycles there will be no visible performance degradation.

Another system aspect that was investigated concerns the generated heat from the SMA actuators and its effect on the overall temperature of the hand prosthesis. Experimental results showed that the maximum temperature recorded by the temperature sensor on the MCB during performance of all its common grip patterns did not exceed the room temperature by more than 5°C. Since the recorded temperature of the MCB is very close to the AUs, the expected temperature of the outer surface of the prosthetic hand is much lower. In fact, this value was measured via a laser-sighted infrared gun−style thermometer (Pro Exotics PE-2), and it was found that, for the closest to the AUs outer surfaces, there was no more than 1°C temperature rise, even after three minutes of consecutive open/close hand movements.

As it was expected, the power consumption of the developed device is relatively high due to the

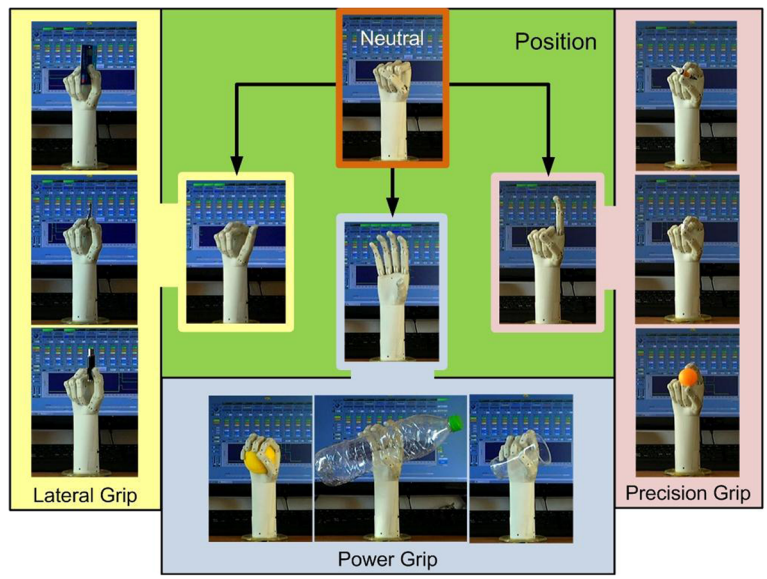

Fig. 43 Sequence of movements for lateral, power and precision grips of various objects (lateral grip: credit card, key, USB stick; power grip: sponge ball (68 mm diameter), plastic bottle (81.5 mm diameter), plastic cup (diameter varying from 50 to 67 mm); precision grip: glue tube, dice, table tennis ball (38 mm diameter)). "Neutral" and "Position" refers to the resting and pre-grasp posture of the prosthetic hand, respectively. A related video is included in the supplementary content (Online Resource 1)

low energy efficiency of the SMAs and the lack of back-lock mechanisms. For example, its maximum power consumption in a power grip, wherein five SMA actuator wires are simultaneously powered for the extension of all the digits, is about 140 W, which is about four times higher than that of the commercial prostheses (e.g. the i-Limb hand has a maximum wattage of 37 W [10]). Although this value looks too large to cope with a portable battery, it only concerns the time needed for the digits to reach their stretched out positions; then, as previously shown, significantly less power consumption is typically used for maintaining the hand posture (about 50 W). Moreover, given the passive adaptive grip provided from the bias springs, the energy requirements of the developed hand can be further reduced. Taking also into consideration the rapid progress of the batteries field and the recent breakthroughs [74], power consumption of the hand prosthesis will soon be a trivial issue to address. Based on the current available battery technology, it is estimated that a standard 3-cell rechargeable battery of 11.1 V / 2.7 Ah (e.g. a Lithium-Polymer battery weighing about 180 grams) would be sufficient for producing over 300 basic grasps (whereof 35 % power, 30 % precision and 20 % lateral [11]) per charge. A battery of higher capacity can also be used, if this is not integrated in the envelope of the prosthetic socket but mounted externally at the upper arm, in order to have more available grasps per charge without causing user discomfort symptoms due to its weight.

5 Conclusions and Future Work

In this research paper, an innovative SMA actuated prosthetic hand was presented. A summary of its technical specifications can be found in Table 3. By utilizing custom-made compact actuation units with SMA wires instead of traditional electric motors, certain attractive characteristics are introduced to the proposed hand prosthesis. More specifically, compared to the current most advanced commercial prosthetic hands, the developed SMA actuated device presents an about 30 % weight reduction, while also being totally silent, and thus eliminating some of the major causes of user discomfort and prosthesis rejection. Furthermore, the comparatively low cost of these actuator wires in combination with the decreasing costs of the additive manufacturing enables the development of low-cost prosthetic devices that will be accessible even to those upper limb amputees without insurance or monetary means. All these benefits come at the costs of higher power consumption and relatively low grip forces.

Table 3 Technical specifications of the developed hand

Number of digits	5 (4 fingers + thumb)
Number of DOFs	15 (11 active + 4 passive)
Number of actuators	9
Type of actuators	One-way SMA wires
Type of transmission	Nylon-coated stainless steel cables
Operating noise	0 dB
Hand opening	135.8 mm
Min. open/close time	1.6 s / 2.1 s
Total mass	0.31 kg (w/o battery, cosmesis)
Size	Average human hand
Max. grip load	1.5 kg
Max. wattage (peak/typical)	140 W / 50 W

Exploiting the self-sensing capabilities of the SMAs, a new position controller was developed and tested based on the electrical resistance feedback. Despite the non-linear nature of the SMA response, the devised controller showed stable and accurate positioning of the hand digits without the need for additional position sensors and hence additional costs. Moreover, future integration of higher-precision electronics for more accurate resistance measurements is expected to improve position control of the digits and reduce the amount of generated heat; as a consequence, the speed and efficiency of the proposed device are also expected to be improved.

Some initial grasp experiments of everyday objects were carried out to evaluate the functionality of the proposed device. As it was demonstrated, the hand proved competent to perform the three most common grip patterns (power, precision, lateral) with an acceptable speed (open/close time). In the future, further experiments will be conducted in order to evaluate the grasp stability and robustness against disturbances. Future work will also examine the hand performance in other grasp types, such as hook and tripod grip, both on the bench and in the clinic. The clinical evaluation in real use conditions is planned to be conducted utilizing an intuitive EMG control strategy. In these trials,

the role of the tactile sensors and feedback devices in hand control will also be investigated.

Acknowledgments This research has been co-financed by the European Union (European Social Fund – ESF) and Greek national funds through the Operational Program "Education and Lifelong Learning" of the National Strategic Reference Framework (NSRF) - Research Funding Program: Heracleitus II. Investing in knowledge society through the European Social Fund [grant number D.276.001.096].

References

1. Rosa, A.D.L., Walker, G.R.L., Goldsmith, J.B., Elias, J.H., Godden, M.P., Greenhill, R.M.: Robotic hand. US Patent 2011/0040408 A1
2. Grebenstein, M., Chalon, M., Friedl, W., Haddadin, S., Wimböck, T., Hirzinger, G., Siegwart, R.: The hand of the DLR hand arm system: Designed for interaction, Vol. 31 (2012)
3. Bridgwater, L.B., Ihrke, C.A., Diftler, M.A., Abdallah, M.E., Radford, N.A., Rogers, J.M., Yayathi, S., Askew, R.S., Linn, D.M.: The Robonaut 2 hand - designed to do work with tools. In: 2012 IEEE International Conference on Robotics and Automation (ICRA) Saint Paul, pp. 3425–3430. Minnesota (2012)
4. Kyberd, P.J., Gow, D., Chappell, P.H.: Research and the future of myoelectric prosthetics. In: Muzumdar, A. (ed.): Prostheses, Powered Upper Limb, pp. 175-190. Springer, Berlin Heidelberg (2004)
5. Pons, J.L., Rocon, E., Ceres, R., Reynaerts, D., Saro, B., Levin, S., Moorleghem, W.V.: The MANUS-HAND dextrous robotics upper limb prosthesis: Mechanical and manipulation aspects. Autonom. Robots **16**, 143–163 (2004)
6. Kargov, A., Ivlev, O., Pylatiuk, C., Asfour, T., Schulz, S., Gräser, A., Dillmann, R., Bretthauer, G.: Applications of a fluidic artificial hand in the field of rehabilitation. In: Kommu, S.S. (eds.) Rehabilitation Robotics, p. 648. Itech Education and Publishing, Vienna (2007)
7. Biddiss, E., Beaton, D., Chau, T.: Consumer design priorities for upper limb prosthetics. Disabil. Rehabil. Assist. Tech. **2**(6), 346–357 (2007)
8. Pylatiuk, C., Schulz, S., Doderlein, L.: Results of an internet survey of myoelectric prothetic hand users. Prosthetics Orthot. Int. **31**(4), 362–370 (2007)
9. Dechev, N., Cleghorn, W.L., Naumann, S.: Thumb design of an experimental prosthetic hand. In: International Symposium On Robotics and Automation, pp. 7–12. Monterrey (2000)
10. Touch Bionics, Inc.: i-Limb Ultra Revolution data sheet
11. Cipriani, C., Controzzi, M., Carrozza, M.C.: The SmartHand transradial prosthesis. J. Neuro Eng. Rehab. **8**(29), 1–13 (2011)
12. Evans, C.O., Perry, N.C., Van Der Merwe, D.A., Violette, K.D., Coulter, S.M., Doyon, T.A., Blumberg, J.R.D.: Arm prosthetic device. US Patent 2011/0257765 A1
13. Schulz, S., Pylatiuk, C., Bretthauer, G.: A new ultralight anthropomorphic hand. In: 2001 IEEE International Conference on Robotics and Automation (ICRA), vol. 2433, pp. 2437–2441. Seoul (2001)
14. Cura, V.O.D., Cunha, F.L., Aguiar, M.L., Cliquet, A.J.r.: Study of the different types of actuators and mechanisms for upper limb prostheses. Artif. Organs **27**(6), 507–516 (2003). doi:10.1046/j.1525-1594.2003.07000.x
15. Love, L.J., Lind, R.F., Jansen, J.F.: Mesofluidic actuation for articulated finger and hand prosthetics. In: 2009 IEEE/RSJ International Conference on Intelligent Robots and Systems (IROS). St. Louis (2009)
16. Kumar, P.K., Lagoudas, D.C.: Introduction to shape memory alloys. In: Lagoudas, D.C. (eds.) Shape Memory Alloy Modelling and Engineering Applications, pp. 1–51. Springer, New York (2008)
17. Mavroidis, C., Pfeiffer, C., Mosley, M.J.: Conventional actuators, shape memory alloys, and electrorheological fluids. In: Bar-Cohen, Y. (ed.) Automation, Miniature Robotics & Sensors for Non-Destructive Testing & Evaluation. pp. 189–214. The American Society for Nondestructive Testing, Inc. (ASNT) (2000)
18. DeLaurentis, K.J., Mavroidis, C.: Mechanical design of a shape memory alloy actuated prosthetic hand. Tech Health Care **10**(1), 91–106 (2002)
19. DeLaurentis, K.J., Mavroidis, C.: Rapid fabrication of a non-assembly robotic hand. Assem Autom **24**(4), 394–405 (2004)
20. Maeno, T., Hino, T.: Miniature five-fingered robot hand driven by shape memory alloy actuators. In: 12th IASTED International Conference, pp. 174–179. Honolulu (2006)
21. Cho, K.-J., Rosmarin, J., Asada, H.: SBC hand: a lightweight robotic hand with an SMA actuator array implementing C-segmentation. In: 2007 IEEE International Conference on Robotics and Automation (ICRA), pp. 921–926 (2007)
22. Jung, S., Bae, J., Moon, I.: Lightweight prosthetic hand with five fingers using SMA actuator. In: 11th International Conference on Control, Automation and Systems (ICCAS) Gyeonggi-do, pp. 1797–1800. Korea (South) (2011)
23. Lee, J.H., Okamoto, S., Matsubara, S.: Development of multi-fingered prosthetic hand using shape memory alloy type artificial muscle. Comput. Technol. Appl. **3**(7), 477–484 (2012)
24. Bundhoo, V.: Design and evaluation of a shape memory alloy-based tendon-driven actuation system for biomimetic artificial fingers, Thesis, University of Victoria (2009)
25. Saether, O.F.: Flexinol as actuator for a humanoid fingerpossibilities and challenges. Thesis, University of Oslo (2008)
26. Lan, C.-C., Yang, Y.-N.: An analytical design method for a shape memory alloy wire actuated compliant finger. In: ASME 2008 International Design Engineering Technical Conferences (IDETC) & Computers and Information in Engineering Conference (CIE), vol. 3–6, pp. 1–10. Brooklyn (2008)
27. Ahmed, M.A., Taher, M.F., Metwalli, S.M.: Shape memory alloy actuator system optimization for new hand prostheses World Academy of Science. Eng. Technol. **61**(188), 1021–1026 (2012)

28. Loh, C.S., Yokoi, H., Arai, T.: New shape memory alloy actuator: Design and application in the prosthetic hand. In: 27th Annual International Conference of the IEEE Engineering in Medicine and Biology Society (EMBS). Shanghai (2005)
29. Yang, K., Wang, Y.: Design, drive and control of a novel SMA-actuated humanoid flexible gripper. J. Mech. Sci. Technol. **22**, 895–904 (2008)
30. Price, A.D., Jnifene, A., Naguib, H.E.: Design and control of a shape memory alloy based dexterous robot hand. Smart Mater. Struct. **16**(4), 1401–1414 (2007)
31. Dilibal, S., Guner, E., Akturk, N.: Three-finger SMA robot hand and its practical analysis. Robotica **20**, 175–180 (2002). doi:10.1017/S0263574701003757
32. Andrianesis, K., Tzes, A., Kolyvas, E., Koveos, Y.: Biomimetic actuation and control of an anthropomorphic finger. Int. Rev. Mech. Eng. (IREME) **2**(1), 163–171 (2008)
33. Andrianesis, K., Tzes, A.: Design of an anthropomorphic prosthetic hand driven by shape memory alloy actuators. In: 2nd IEEE RAS/EMBS International Conference Biomedical Robotics and Biomechatronics (BioRob), pp. 517–522. Scottsdale (2008)
34. Andrianesis, K., Koveos, Y., Nikolakopoulos, G., Tzes, A.: Experimental study of a shape memory alloy actuation system for a novel prosthetic hand. In: Cismasiu, C. (ed.) Shape Memory Alloys, pp. 81-106. InTech (2010)
35. Andrianesis, K., Tzes, A.: Design of an innovative prosthetic hand with compact shape memory alloy actuators. In: 21st Medit. Conference Control and Automation (MED), Platanias-Chania, Crete (2013)
36. Jones, L.A., Lederman, S.J.: Human hand function. Oxford University Press, Inc., New York (2006)
37. Banks, J.L.: Design and control of an anthropomorphic robotic finger with multi-point tactile sensation. Thesis, Massachusetts Institute of Technology (2001)
38. Hollister, A., Buford, W.L., Myers, L.M., Giurintano, D.J., Novick, A.: The axes of rotation of the thumb carpometacarpal joint. J. Orthop. Res. **10**(3), 454–460 (1992)
39. LaViola, J.J. Jr.: A survey of hand posture and gesture recognition techniques and technology. In: vol. CS-99-11. Brown University, Providence (1999)
40. Feix, T.: Anthropomorphic hand optimization based on a latent space analysis, Thesis, Technical University of Vienna (2011)
41. Henderson, A., Pehoski, C.: Hand function in the child: Foundations for remediation. Mosby, St. Louis, Missouri (2006)
42. NASA: Anthropometry and biomechanics. In: Man-systems integration standards, vol. 1. vol. 3 (1995)
43. Weir, R.F., Sensinger, J.W.: The design of artificial arms and hands for prosthetic applications. In: Kutz, M. (ed.) Biomedical Engineering and Design Handbook, pp. 537–598. McGraw-Hill, New York (2009)
44. Sangole, A.P., Levin, M.F.: Arches of the hand in reach to grasp. J. Biomech. **41**(4), 829–837 (2008)
45. Gosselin, C., Pelletier, F., Laliberte, T.: An anthropomorphic underactuated robotic hand with 15 Dofs and a single actuator. In: IEEE International Conference on Robotics and Automation (ICRA), pp. 19–23. Pasadena (2008)
46. Birglen, L., Laliberté, T., Gosselin, C.: Design and control of the Laval underactuated hands. In: Underactuated Robotic Hands. Springer Tracts in Advanced Robotics, vol. 40, pp. 171–207. Berlin Heidelberg, Springer (2008)
47. Birglen, L., Laliberté, T., Gosselin, C.: Grasping vs. manipulating. In: Underactuated Robotic Hands, vol. 40, pp. 7–31. Springer Berlin, Heidelberg, Berlin (2008)
48. Buchholz, B., Armstrong, T.J., Goldstein, S.A.: Anthropometric data for describing the kinematics of the human hand. Ergonomics **35**(3), 261–273 (1992). doi:10.1080/00140139208967812
49. Gómez, G., Hernandez, A., Hotz, P.E.: An adaptive neural controller for a tendon driven robotic hand. In: Arai, T. (ed.) 9th International Conference on Intelligent Autonomous Systems (IAS), pp. 298-307. Tokyo, IOS Press (2006)
50. Palm, W.: Rapid prototyping primer. In: vol. 2/4/2010. Penn State Learning Factory (1998)
51. Martin, T.B., Ambrose, R.O., Diftler, M.A., Platt, R. Jr., Butzer, M.J.: Tactile gloves for autonomous grasping with the NASA/DARPA Robonaut. In: 2004 IEEE International Conference on Robotics and Automation (ICRA), vol. 1712, pp. 1713–1718. New Orleans
52. Evanczuk, S.: Fundamentals of temperature-sensing devices (2011)
53. Mohd Jani, J., Leary, M., Subic, A., Gibson, M.A.: A review of shape memory alloy research, applications and opportunities. Mater. Des. **56**(0), 1078–1113 (2014). doi:10.1016/j.matdes.2013.11.084
54. In: Smith, D.G., Michael, J.W., Bowker, J.H. (eds.): Atlas of Amputations and Limb Deficiencies, 3rd edn. American Academy of Orthopaedic Surgeons (2004)
55. In: Muzumdar, A. (ed.): Powered Upper Limb Prostheses: Control, Implementation and Clinical Application, 1st edn. Springer, New York (2004)
56. Madden, J.D.W., Vandesteeg, N.A., Anquetil, P.A., Madden, P.G.A., Takshi, A., Pytel, R.Z., Lafontaine, S.R., Wieringa, P.A., Hunter, I.W.: Artificial muscle technology: Physical principles and naval prospects. IEEE J. Ocean. Eng. **29**(3), 706–728 (2004). doi:10.1109/joe.2004.833135
57. Uustal, H., Baerga, E.: Prosthetics and orthotics. In: Cuccurullo, S.J. (ed.) Physical Medicine and Rehabilitation Board Review. Demos Medical Publishing, New York (2004)
58. Dynalloy, Inc.: Technical Characteristics of Flexinol Actuator Wires (2010)
59. Abolfathi, P.P.: Development of an Instrumented and Powered Exoskeleton for the Rehabilitation of the Hand, Thesis, University of Sydney (2007)
60. MacGregor, R.: Shape memory alloy actuators and control methods. US Patent 6,574,958 (2003)
61. Belter, J.T., Dollar, A.M.: Performance characteristics of anthropomorphic prosthetic hands. In: 2011 IEEE International Conference on Rehabilitation Robotics (ICORR), ETH Zurich, pp. 921–927. Switzerland (2011)
62. Teh, Y.H., Featherstone, R.: An architecture for fast and accurate control of shape memory alloy actuators. Int. J. Robot. Res. **27**(5), 595–611 (2008). doi:10.1177/0278364908090951
63. Ma, N., Song, G., Lee, H.-J.: Position control of shape memory alloy actuators with internal electrical resistance feedback using neural networks. Smart Mater. Struct. **13**(4), 777–783 (2004). doi:10.1088/0964-1726/13/4/015
64. Chatterjee, A., Aggarwal, V., Ramos, A., Acharya, S., Thakor, N.V.: A brain-computer interface with vibrotactile

biofeedback for haptic information. J. NeuroEngineering Rehabil. **4**(40) (2007)
65. Davalli, A., Sacchetti, R., Fanin, S., Avanzolini, G., Urbano, E.: Biofeedback for upper limb myoelectric prostheses. Technol. Disabil. **13**, 161–172 (2000)
66. Engeberg, E.D., Meek, S.: Enhanced visual feedback for slip prevention with a prosthetic hand. Prosthetics Orthot. Int. **36**(4), 423–429 (2012). doi:10.1177/0309364612440077
67. Sapsanis, C., Georgoulas, G., Tzes, A., Lymberopoulos, D.: Improving EMG based Classification of basic hand movements using EMD. In: 35th Annual International Conference of the IEEE Engineering in Medicine and Biology Society (EMBC), pp. 5754–6757. Osaka
68. Lake, C., Dodson, R.: Progressive upper limb prosthetics. Phys. Med. Rehabil. Clinics N. Am. **17**(1), 49–72 (2006)
69. Cocaud, C., Price, A., Jnifene, A., Naguib, H.: Position control of an experimental robotic arm driven by artificial muscles based on shape memory alloys. Int. J. Mech. Mater. Des. **3**(3), 223–236 (2006)
70. Ashrafiuon, H., Eshraghi, M., Elahinia, M.H.: Position control of a three-link shape memory alloy actuated robot. J. Intell. Mater. Syst. Struct. **17**(5), 381–392 (2006)
71. Rezaeeian, A., Yousefi-Koma, A., Shasti, B., Doosthoseini, A.: ANFIS modeling and feedforward control of shape memory alloy actuators, Vol. 2 (2008)
72. Cho, K.-J., Asada, H.: Architecture design of a multi-axis cellular actuator array using segmented binary control of shape memory alloy. IEEE Trans. Robot. **22**(4), 831–843 (2006)
73. Zecca, M., Roccella, S., Cappiello, G., Ito, K., Imanishi, K., Miwa, H., Carrozza, M.C., Dario, P., Takanishi, A.: From the human hand to a humanoid hand: Biologically-inspired approach for the development of Robocasa Hand #1. In: Zielinska, T., Zielinski, C. (eds.) 16th CISM-IFToMM RoManSy Symposium, pp. 287–294. Warsaw, Springer
74. Pikul, J.H., Gang Zhang, H., Cho, J., Braun, P.V., King, W.P.: High-power lithium ion microbatteries from interdigitated three-dimensional bicontinuous nanoporous electrodes. Nat. Commun. **4**, 1732 (2013). doi:10.1038/ncomms2747